HHS Public Access

Author manuscript

Nat Commun. Author manuscript; available in PMC 2014 February 13.

Published in final edited form as:

Nat Commun. 2013 ; 4: 3000. doi:10.1038/ncomms4000.

The atypical mechanosensitive microRNA-712 derived from pre-ribosomal RNA induces endothelial inflammation and atherosclerosis

Dong Ju Son[1,2,*], **Sandeep Kumar**[1,2,*], **Wakako Takabe**[1,2], **Chan Woo Kim**[1,2,3], **Chih-Wen Ni**[1], **Noah Alberts-Grill**[2], **In-Hwan Jang**[1], **Sangok Kim**[4], **Wankyu Kim**[4], **Sang Won Kang**[4], **Andrew H. Baker**[5], **Jai Woong Seo**[6], **Katherine W. Ferrara**[6], and **Hanjoong Jo**[1,2,3,¶]

[1]Wallace H. Coulter Department of Biomedical Engineering, Georgia Institute of Technology and Emory University, Atlanta

[2]Division of Cardiology, Department of Medicine, Emory University, Atlanta, GA, USA

[3]Department of Bioinspired Science, Ewha Womans University, Seoul, South Korea

[4]Department of Life Science, Ewha Womans University, Seoul, South Korea

[5]Institute of Cardiovascular and Medical Sciences, University of Glasgow, Glasgow, UK

[6]Department of Biomedical Engineering, University of California, Davis, CA, USA

Abstract

MicroRNAs (miRNAs) regulate cardiovascular biology and disease, but the role of flow-sensitive microRNAs in atherosclerosis is still unclear. Here we identify miRNA-712 (miR-712) as a mechanosensitive miRNA upregulated by disturbed flow (*d-flow)* in endothelial cells, *in vitro* and *in vivo.* We also show that miR-712 is derived from an unexpected source, pre-ribosomal RNA, in an exoribonuclease-dependent but DiGeorge Syndrome Critical Region-8 (DGCR8)-independent manner, suggesting that it is an atypical miRNA. Mechanistically, *d-flow*-induced miR-712 downregulates tissue inhibitor of metalloproteinase-3 (TIMP3) expression, which in turn activates the downstream matrix metalloproteinases (MMPs) and a disintegrin and metalloproteases (ADAMs) and stimulate pro-atherogenic responses, endothelial inflammation and permeability.

¶Address for Correspondence: Hanjoong Jo, PhD, Wallace H. Coulter Department of Biomedical Engineering, Georgia Institute of Technology and Emory University, Health Sciences Research Building, E170, Atlanta, Georgia 30322, hanjoong.jo@bme.gatech.edu, Telephone: 404-712-9654, Fax: 404-727-3330.

*Contributed equally to this work.

Author Contribution

DJS and SK contributed equally to the manuscript. DJS, SK, WT, CN, JWS and KWF designed the experiments. DJS, SK, WT, CN, CW, JWS, SK, IHJ and NAG performed the experiments. DJS, WT, SK, CN, CWK, SOK, WKK, JWS, and NAG analyzed the data. AHB and KWF provided key reagents. SK, DJS, and HJ wrote the manuscript. HJ supervised the overall research, secured funding, designed experiments and interpreted results and wrote the manuscript.

Accession codes

The microarray data have been deposited in NCBI's Gene Expression Omnibus (GEO) and are accessible through GEO Series accession number GSE52243.

Conflict of Interest

None.

Furthermore, silencing miR-712 by anti-miR-712 rescues TIMP3 expression and prevents atherosclerosis in murine models of atherosclerosis. Finally, we report that human miR-205 shares the same “seed sequence” as murine-specific miR-712, and also targets TIMP3 in a flow-dependent manner. Targeting these mechanosensitive “athero-miRs” may provide a new treatment paradigm in atherosclerosis.

Introduction

Atherosclerosis is the major underlying cause of cardiovascular pathologies and preferentially occurs in arterial regions exposed to disturbed flow (*d-flow*) by altering the gene expression[1, 2, 3, 4]. Vascular endothelial cells respond to blood flow through mechanosensors which transduce the mechanical force associated with flow (known as shear stress) into cell signaling events and changes in gene expression[5, 6, 7]. *D-flow* and stable flow (*s-flow)* promotes and inhibits atherogenesis, respectively, in large part by regulating discrete sets of pro-atherogenic and atheroprotective genes[1, 8, 9]. While *s-flow* upregulates atheroprotective genes such as *Klf2*, *Klf4*, and *eNOS*, *d-flow* upregulates a number of pro-atherogenic genes including vascular cell adhesion molecule-1 (*VCAM-1*)[1, 10] and matrix metalloproteinases (*MMPs*)[11] which mediate pro-angiogenic, pro-inflammatory, proliferative, and pro-apoptotic responses, promoting atherosclerosis[5, 12, 13]. The ways in which the mechanosensitive machinery in endothelial cells regulates gene expression and contributes to these pro-atherogenic events is still poorly understood, especially in the *in vivo* setting. MicroRNAs (miRNAs) are small non-coding RNA molecules that modulate the stability and/or the translational efficiency of its target messenger RNAs (mRNA). miRNAs have been demonstrated to be involved in key physiological and pathophysiological aspects of cardiovascular biology but the role of flow-sensitive miRNAs in atherosclerosis is still unclear.

To address this knowledge gap, we recently developed a mouse model of flow-induced atherosclerosis by partially ligating the left carotid artery (LCA) of the *ApoE*$^{-/-}$ mouse[10]. This model directly demonstrates the causal relationship between *d-flow* and atherosclerosis as the LCA rapidly develops robust atherosclerosis within two weeks following partial ligation that causes *d-flow* with characteristic low and oscillatory shear stress (OS), while the contralateral, undisturbed right common carotid artery (RCA) remains healthy[10] (Figure 1a). In addition, we developed a method of isolating intimal RNA from mouse carotid artery following ligation[1, 10]. This method allows easy and rapid endothelial-enriched RNA isolation that is virtually free of contamination from the vascular smooth muscle cells (VSMCs) and leukocytes. Using this mouse model and the RNA isolation method, we identified more than 500 mechanosensitive genes, including novel ones such as *lmo4*, *klk10*, and *dhh*, and confirming well-known mechanosensitive genes, such as *VCAM-1*, *klf2* and *eNOS*[1]. In this study, we used this model to identify mechanosensitive miRNAs regulated by *d-flow* and their role in endothelial inflammation and atherosclerosis.

Here we identify miR-712 as the most flow-sensitive miRNA that is upregulated by *d-flow* in endothelial cells, *in vivo* and *in vitro*. Further, we identified a novel miRNA biogenesis mechanism from RN45S gene in a noncanonical manner. Further studies identify tissue

inhibitor of metalloproteinase 3 (TIMP3) as a direct target of miR-712 which induces endothelial inflammation and atherosclerosis. Treatment with specific antagonist of miR-712 (anti-miR-712) inhibits endothelial inflammation, barrier function and atherosclerosis in a TIMP3-dependent manner. Collectively, our results suggest that targeting the mechanosensitive miRNAs by their anti-miRs may provide a novel potential therapeutic approach to treat atherosclerosis.

Results

miR-712 is a flow-sensitive microRNA upregulated by *d-flow*

To identify mechanosensitive miRNAs in arterial endothelium *in vivo*, we carried out miRNA array analyses using endothelial-enriched RNAs from partially ligated mouse carotids (Figure 1a) as in our prior analyses of mechanosensitive mRNAs[1] and integrated these two genome-wide data-sets using a systems biology approach to help us identify relevant miRNA-target gene connections.

The *in vivo* microarray data showed that 45 (27 up- and 18 downregulated) miRNAs were altered by more than 50% in the LCA endothelium compared to the RCA at 12 and 48 hours post-ligation (Figure 1b and Supplementary Figure S1a and Supplementary Table S1). Quantitative PCR (qPCR) using additional independent RNA samples was used to validate the miRNA array data for the top 10 most mechanosensitive miRNAs (5 up-, 5 down-regulated miRNAs at 48 hours post-ligation): upregulated (miR-330*, 712, 699, 223 and 770–5p) and down-regulated (miR-195, 30c, 29b, 26b and let-7d) miRNAs (Figure 1 c and d; Supplementary Figure S1b). To determine whether these mechanosensitive miRNAs that were identified *in vivo* responded specifically to shear stress, we tested expression of these miRNAs *in vitro* using immortalized mouse aortic endothelial cells (iMAECs) that were subjected to laminar (LS) or OS, mimicking *s-flow* and *d-flow in vivo*, respectively[14] (Figure 1e). These results showed that miR-712 was the most consistently and robustly upregulated miRNA both *in vivo* and under flow conditions *in vitro*, leading us to further characterize its expression and function.

A time-course study showed that miR-712 was upregulated significantly in the *d-flow* region (LCA) compared to *s-flow* region (RCA) at 48 h post-ligation in mouse carotids (Figure 2a). Using the miScript qPCR assay that can distinguish between the pre-miR and mature forms of miR-712, we found that pre-miR-712 expression significantly increased at 48 h post-ligation while expression of mature-miR-712 increased significantly in LCA at 24 and 48 h post-partial ligation (Figure 2b and c), which was subsequently validated by sequencing the PCR amplicons (data not shown). This suggests that *d-flow* initially stimulate processing of pre-existing miR-712 precursor form into the mature form within 24h, which is then followed by biogenesis of pre-miR-712 and its concurrent processing to the mature form later on, in mouse artery *in vivo*.

Exposure of iMAECs to OS for 24 h *in vitro* also dramatically increased expression of mature and precursor forms of miR-712 compared to LS as determined by qPCR (Figure 2d and e) and Northern blot (Supplementary Figure S2), confirming the flow-sensitivity of miR-712. Studies using *in situ* hybridization with a miR-712 probe (Exiqon) showed

significantly increased expression of miR-712 in the LCA endothelium, compared to the RCA (Figure 2f lower panel), further validating the *in vivo* microarray and qPCR results. To rule out whether increased expression of miR-712 in LCA was not simply due to an acute change in mechanical environment created by the partial ligation surgery, we tested expression of miR-712 in mouse aortic arch, where the atherosclerosis-prone lesser curvature (LC) and athero-protected greater curvature (GC) are naturally and chronically exposed to *d-flow* and *s-flow*, respectively (Figure 1a). Expression of miR-712 was significantly higher in the flow-disturbed LC compared to GC (Figure 2f, upper panel; Supplementary Figure S3). This result was further corroborated by qPCR assay using endothelial-enriched RNA obtained from the LC and GC regions of aortic arch (Supplementary Figure S4). Interestingly, we also found that miR-712 expression was increased in the plasma of mice that underwent partial carotid ligation but not in shams (Supplementary Figure S5). These findings suggest that miR-712 is indeed a flow-sensitive miRNA, which is significantly upregulated in endothelial cells exposed to *d-flow* in the aortic arch naturally or in LCA upon partial carotid ligation, as well as *in vitro.*

miR-712 is generated from RN45S gene in an atypical manner

The genomic locus and biogenesis pathway of miR-712 were not known. Our nucleotide sequence search revealed that the pre-miR-712 sequence matched to the internal transcribed spacer region 2 (ITS2) region of the murine pre-ribosomal RNA, *RN45s* gene (Figure 2g), which is still not completely annotated. The RN45S encodes for 45S, which contains sequences for 18S, 5.8S and 28S rRNAs along with two intervening spacers, ITS1 and ITS2 (Figure 2g). Since ribosomal RNAs have never been reported to be a source of miRNAs, we examined whether miR-712 biogenesis was regulated by the canonical pathway using the DiGeorge Syndrome Critical Region 8 (DGCR8)/DROSHA and DICER microRNA processors[15, 16, 17] or by non-canonical pathways[18, 19] in a flow-dependent manner. Expression of DICER1 and DGCR8 was not altered by flow in endothelial cells *in vitro* (iMAEC) and *in vivo* (mouse carotids and aortic arch) (Figure 2h and i, Supplementary Figure S6a and b). Since, XRN1 is an exonuclease that is known to degrade the ITS2 region during the processing of *RN45S*[20], we tested whether XRN1 is shear-dependent and regulates biogenesis of miR-712. We found that XRN1 expression was downregulated by *d-flow* in the mouse carotid (Figure 2j) and aortic arch (Supplementary Figure S6c) and in human and mouse endothelial cells *in vitro* (Figure 2k and l). Further, knockdown of XRN1 by siRNA treatment increased the expression of miR-712, suggesting that reduction of XRN1 under *d-flow* conditions led to accumulation of miR-712 (Figure 2m and Supplementary Figure S6d and S7a). In contrast, knockdown of the canonical miRNA processor DGCR8 did not affect miR-712 expression (Figure 2m and Supplementary Figure S6e and S7). These results suggest that miR-712 is a murine-specific, non-canonical miRNA derived from an unexpected source, pre-ribosomal RNA, in a XRN1-dependent, but DGCR8-independent and DICER1-dependent manner.

To test whether this novel mechanism of miRNA biogenesis from pre-ribosomal RNA exists in humans as well, we examined human *RN45S* gene for putative miRNAs using a computational predication program, miREval[21, 22]. This search revealed that human-specific miR-663 could be derived from *RN45s* gene (Figure 2g), in addition to its previously

annotated genomic locus on chromosome 2 (miRBase). Interestingly, like miR-712, miR-663 was previously identified from a microarray study as one of the most shear-sensitive miRNAs in human endothelial cells and was shown to induce endothelial inflammation, a key atherogenic step[14], raising a possibility that they share a common biogenesis pathway and roles in endothelial function. Consistent with this hypothesis, we found that XRN1 expression is inhibited by OS (Figure 2l) and that siRNA knockdown of XRN1 significantly increased miR-663 expression in human endothelial cells (Supplementary Figure S6f and g).

miR-712 targets TIMP3 in the endothelium

Through *in silico* analysis using miR-712 predicted target gene list from TargetScan and the mechanosensitive gene list using the same mouse model[1], we identified *TIMP3* as a potential gene target. TIMP3 was selected for further study since the miR-712 interactome analysis (Figure 3a; Supplementary Figure S8) suggested its potential role as a key gene hub connected to numerous genes of interest, including matrix metalloproteinases-2/9 (*MMP2/9*) and a disintegrin and metalloproteinase 10/17 (*ADAM10/17*), ADAM with thrombospondin type 1 motif, 4 (*ADAMTS4*) and *versican* that are known to play a critical role in the regulation of vascular inflammation, permeability and atherosclerosis[23, 24, 25, 26, 27, 28].

To test whether miR-712 targets *TIMP3* in endothelial cells (Figure 3b), we employed a dual luciferase reporter assay in iMAECs transfected with either wild-type or mutated *TIMP3* 3′-UTR firefly luciferase constructs. Treatment of cells with pre-miR-712 inhibited luciferase activity in a dose-dependent manner, while mutant or control pre-miR had no effect (Figure 3c), demonstrating that miR-712 binds to the *TIMP3* 3′-UTR and inhibits its expression in endothelial cells.

Next, we tested whether *TIMP3* expression was regulated by flow in a miR-712-dependent manner. Exposure of iMAECs to OS for 24 h significantly decreased TIMP3 mRNA and protein expression, compared to LS (Figure 3d and e). Pre-miR-712 treatment decreased expression of *TIMP3* in LS-exposed cells (Figure 3f), while inhibition of miR-712 using locked nucleic acid (LNA)-based anti-miR-712 increased TIMP3 expression in cells exposed to OS (Figure 3g). These findings demonstrate that miR-712 upregulated by OS, is directly responsible for the loss of *TIMP3* expression in endothelial cells.

To examine the biological relevance of reduced TIMP3 by miR-712, we tested TNFα-converting enzyme (TACE/ADAM17) activity by measuring soluble-TNFα released in to the conditioned medium by treating cells with pre-miR-712 vs. anti-miR-712 or siTIMP3 vs. TIMP3 overexpression vector in iMAECs under static or shear conditions. We found that soluble-TNFα release into the conditioned medium was increased by OS (Figure 4a) which was inhibited by anti-miR-712 treatment or TIMP3 overexpression (Figure 4b; Supplementary Figure S9). In contrast, pre-miR-712 treatment or TIMP3 knockdown increased release of soluble-TNFα into the conditioned media in static and LS exposed cells (Figure 4b; Supplementary Figure S9). These results suggest that ADAM17/TACE activity was regulated by OS in a miR-712 and TIMP3-dependent manner. In addition, endothelial inflammation was increased by pre-miR-712 as measured by monocyte (J774.1 cells) adhesion to endothelium (Figure 4c). Furthermore, endothelial permeability as determined in

iMAECs using by fluorescent-dextran was also increased by pre-miR-712, which was inhibited by overexpression of TIMP3 (Figure 4d). Taken together, these results indicate that mechanistically TIMP3 is downstream of miR-712 and inhibition of miR-712 by anti-miR-712 treatment or overexpression of TIMP3 can overcome endothelial inflammation induced by *d-flow*.

In vivo delivery of anti-miR-712 to mouse endothelium

To test whether *d-flow*-induced miR-712 plays a key role in atherosclerosis, mice were treated with LNA-based anti-miR-712. First, we found that anti-miRs can be effectively delivered to arterial endothelium *in vivo* as demonstrated by two independent methods: confocal *en face* imaging of TexasRed-labeled control LNA-anti-miR (Figure 5a and Supplementary Figure S10a–d) and autoradiography of ^{64}Cu-labelled anti-miR-712 (Figure 5b and Supplementary Figure S10e–f). Interestingly, both fluorescent-labeled anti-miR and radiolabelled anti-miR preferentially accumulated in the flow-disturbed LCA and aortic arch, which is likely due to increased endothelial mass transfer[29] and permeability to macromolecules in *d-flow* areas[30]. A dose-curve study showed that anti-miR-712 (5 mg/kg, *s.c.*) effectively silenced *d-flow*-induced miR-712 expression in LCA endothelium *as* compared to the mismatched control (Figure 5c), and this dose was used for all subsequent studies. We found that expression of TIMP3 mRNA and protein was reduced in *d-flow* regions both in the partially ligated LCA and aortic arch LC compared to RCA and GC, respectively, and it was rescued by the anti-miR-712 treatment (Figure 5d and Supplementary Figure S11). This further demonstrates the role of miR-712 in regulation of *TIMP3* expression in a flow-dependent manner *in vivo*. Since TIMP3 is a well-known inhibitor of MMPs and ADAMs, we examined the effect of anti-miR-712 on these metalloproteinase activities *in vivo*. MMP activity (*in situ* zymography) and ADAMs activity (versican cleavage by immunohistochemical staining) were increased by *d-flow* in LCA compared to RCA which were significantly blunted by anti-miR-712 treatment (Figure 5e and f). Further, anti-miR-712 treatment inhibited vascular hyperpermeability and junctional VE-cadherin decrease induced by *d-flow* in partially ligated LCA in mouse (Supplementary Figure S12). These *in vivo* results, taken together with the *in vitro* findings shown above, provide strong evidence for a direct hierarchical link between *d-flow*, miR-712, *TIMP3* and its downstream metalloproteinase activity, and endothelial inflammation and barrier dysfunction in arterial wall, which are well-known pro-atherogenic events.

Anti-miR-712 treatment decreases atherosclerotic lesions

Finally, we tested the role of miR-712 in two different models of atherosclerosis using ApoE$^{-/-}$ mice: the partial carotid ligation model fed a high-fat diet that rapidly develops atherosclerosis within 2 weeks[10] and the conventional western diet-fed model that chronically develops atherosclerosis in 3 months[31]. In the carotid ligation model, the LCA rapidly developed atherosclerosis within 2 weeks (Figure 6a) and treatment with anti-miR-712 (5mg/kg, *s.c.* twice a week for 2 weeks) significantly reduced atherosclerosis lesion development and immune cell infiltration compared to the mismatched-anti-miR-712 or saline controls (Figure 6a–e). Similarly, anti-miR-712 treatment (5 mg/kg, *s.c.* twice a week for 3 months) significantly inhibited atherosclerosis development in the conventional

western diet model in whole aortas as well as in the aortic arch (Figure 6f–i). In both models, anti-miR-712 did not affect the serum lipid profile (Supplementary Table S2). These findings demonstrate a potent inhibitory effect of anti-miR-712 in two different murine models of atherosclerosis. In addition, we found that tail-vein injection of recombinant adenoviral TIMP3 (AdTIMP3) significantly increased the expression of TIMP3 in aorta and in blood cells (Supplementary Figure S13) and inhibited atherosclerotic lesion development in the partial carotid ligation model (Figure 6j and k).

Since anti-miR-712 was delivered via *s.c.* injection to mice in our study, anti-miR-712 could affect other tissues and cell types in addition to our primary target, arterial endothelial cells. We found that anti-miR-712 treatment downregulated the miR-712 expression in multiple tissues, including whole blood and spleen (Supplementary Figure S14). Of note, anti-miR-712 treatment significantly inhibited miR-712 expression in blood (Supplementary Figure S14a), which was shown to be increased following partial carotid ligation surgery, but not in sham controls (Supplementary Figure S5). Also, in the arterial wall, expression of miR-712 increased in media and adventitia of the LCA (Supplementary Figure S15). To determine whether miR-712 plays an important role in the media, we performed smooth muscle cell migration and proliferation assays and found that miR-712 stimulated VSMC migration, but not proliferation (Supplementary Figure S16). Taken together, these findings suggest that miR-712 produced in LCA endothelium could be transferred to circulation and adjacent medial smooth muscle cells, contributing to additive proatherogenic effects.

The miR-205 is a potential human homolog of murine mir-712

Since miR-712 is a murine-specific miRNA, we searched whether there are any miR-712 homologs in humans. Using short sequence nucleotide alignment and search tool (BLAST, blast.ncbi.nlm.nih.gov), we found that miR-205 shares the same “seed sequence” with miR-712, and is highly conserved in most vertebrates including humans and mice (Figure 7a). Also, miR-205 and miR-712 share more than 50% of the putative targets (including TIMP3) as shown by the TargetScan analysis (Figure 7b). Importantly, like-miR-712, we found that miR-205 expression (both precursor and mature forms) is higher in iMAECs and human aortic endothelial cells (HAECs) exposed to OS than that of LS (Figure 7c and d). In addition, miR-205 expression was higher in mouse LCA (endothelium as well as media and adventitia) compared to the RCA at 48 h post-partial ligation (Figure 7e). To validate if miR-205 targets TIMP3, we treated iMAECs and HAECs with pre-miR-205 and found that miR-205 downregulates TIMP3 in a concentration-dependent manner (Figure 7f and g). Collectively, these findings suggest that miR-205 shares the seed sequence with miR-712, is also a flow-sensitive miRNA, and targets TIMP3, suggesting that miR-205 is a potential human homolog of murine miR-712.

Discussion

Collectively, our results demonstrate that miR-712 is an atypical mechanosensitive miRNA originating from the RN45S gene and regulates endothelial inflammation and barrier function by targeting TIMP3. We also showed that anti-miR-712 treatment *in vivo* can effectively silence miR-712 expression in arterial endothelial cells, restoring TIMP3 levels

and inhibiting atherosclerotic plaque development in two different murine models of atherosclerosis.

The identification of miR-712 as a flow-dependent miRNA was based on our *in vivo* miRNA microarray study that was carried out using the endothelial-enriched RNA directly from the surgically induced *d-flow* regions of mouse carotid arteries. Endothelial samples from the LC region of aortic arch, where they are naturally and chronically exposed to *d-flow*, also showed increased expression of miR-712, demonstrating that the miR-712 induction in the LCA is not a mere surgical artifact. Further, miR-712 expression was increased in endothelial cells exposed to OS compared to LS, demonstrating its shear sensitivity. Together, these results demonstrate that miR-712 is flow-sensitive miRNA in endothelial cells, both *in vivo* and *in vitro.*

Here, we identified the genomic locus of miR-712 in RN45S gene and its atypical biogenesis mechanism. miR-712 is a murine-specific miRNA and its sequence turns out to be derived from the ITS2 region of mouse RN45S gene. Similarly, we identified that human-specific miR-663 could be derived from the spacer region of human RN45S gene as well. Interestingly, these spacer regions of ribosomal RNA contain species-specific nucleotide sequences that are used as phylogenetic markers[32]. In addition, following the transcription of rRNAs, these spacer regions are rapidly degraded by XRN1 exonuclease[33]. Our data showed that *d-flow* decreased the expression of XRN1 but not the canonical microRNA processors DGCR8/DROSHA in both human and mouse endothelial cells, indicating that there may be a common role of XRN1 in human miR-663 and murine miR-712. Indeed, knockdown of XRN1 significantly increased miR-712 and miR-663 expression while knockdown of DGCR8 did not. These results indicate that miR-712 induction by *d-flow* is dependent on XRN1 but independent of the canonical miRNA processors. This suggests that the novel miRNA biogenesis mechanism using RN45S gene in the XRN1-dependent manner may not exclusive to murine and human species.

It is intriguing that both murine miR-712 and human miR-663 were identified as the most mechanosensitive miRNAs that were upregulated by *d-flow* from two completely independent array studies[14]. These results further support the hypothesis that murine-miR-712 and human miR-663 are derived from their respective *RN45s* genes by a common mechanism involving XRN1 and may serve as pro-atherogenic miRNAs. In this study, we showed how spacer regions of ribosomal RNA can serve as the precursor material for the miRNAs and how knockdown of XRN1 can lead to increased synthesis of the miR-712 in mouse and miR-663 in humans under *d-flow* conditions. To the best of our knowledge, this is the first report demonstrating that miRNAs can be derived from the spacer regions of the rRNAs. Whether XRN1 is directly or indirectly responsible for biogenesis of these atypical miRNAs needs to be further studied.

Here, we showed that miR-712 directly downregulates expression of TIMP3. This is consistent with previous observations that TIMP3 is frequently downregulated in atherosclerosis[34]. TIMP3 is a key hub gene that regulates inflammation, barrier function and extracellular matrix remodeling by inhibiting multiple metalloproteinases such as MMP2/9, ADAM10, ADAMTS4 and ADAM17/TACE that are well-established players in

atherosclerosis[3435]. Our study showed that miR-712 downregulates TIMP3 under *d-flow* conditions leading to activation of MMP2/9 and ADAM activities. MMP2/9 activity was remarkably increased in the LCA which was significantly inhibited by anti-miR-712 treatment. The ADAM-family proteases are known to cleave the extracellular matrix (ECM) proteoglycans such as versican which is known to induce proatherogenic responses including endothelial inflammation[35]. We found increased versican fragmentation by *d-flow* in LCA which was inhibited by anti-miR-712 treatment. In addition, *d-flow* increased endothelial permeability in a manner dependent on miR-712 and TIMP3 which is likely to be mediated by ADAMs such as ADAM17/TACE. ADAM17, which is also known as TACE, induces shedding of membrane-bound TNFα and VE-cadherin leading to soluble-TNFα release and destabilization of junctional integrity[36]. Consistent with this idea, we found that *d-flow* increased soluble-TNFα release *in vitro*, increased endothelial permeability and decreased junctional VE-cadherin expression in LCA (Supplementary Figure S12), which were significantly reversed by anti-miR-712 treatment. Collectively, these findings demonstrate a potent role of miR-712-TIMP3-MMP/ADAM axis induced by *d-flow* on regulation of endothelial inflammation and permeability in the arterial wall.

Since TIMP3 is not likely to be the sole target of miR-712, we attempted to identify additional miR-712 targets in endothelium. We used *in silico* analyses (Supplementary Figure S8), low-density qPCR array of candidate genes and proteomics approach to identify additional miR-712 targets. Unfortunately, in this study, we were unable to validate additional flow-dependent miR-712 targets in endothelial cells. While our results do not rule out the possibility of other target genes, our findings clearly demonstrate the critical role of TIMP3 as the major miR-712 target regulating endothelial inflammation and atherosclerosis.

Several mechanosensitive miRNAs have been identified in endothelial cells but their role in atherosclerosis is still unclear. LS stimulates expression of miR-10a, miR-19a, miR-21, miR-23b, miR-101, and miR-143/145, mediating anti-atherogenic events[37, 38, 39, 40, 41, 42], while OS induces expression of miR-21, miR-92a, and miR-663 leading to proatherogenic responses[14, 43, 44]. miR-155 is also flow-sensitive miRNA but its role in atherosclerosis is controversial[45]. Here we provide evidence that miR-712 is an important mechanosensitive miRNA that is highly upregulated by *d-flow* and plays a critical role in atherosclerosis by affecting endothelial inflammation and barrier function. Using two different murine models of atherosclerosis, we showed that anti-miR-712 treatment prevents atherosclerosis by effectively silencing miR-712 expression thereby restoring TIMP3 activity. We also demonstrated the inhibitory effect of AdTIMP3 on atherosclerosis in partially ligated ApoE$^{-/-}$ mice, further substantiating the role of TIMP3 in flow-induced atherosclerosis.

One caveat of this study is that anti-miR-712 was systemically delivered to mice, and therefore, it is likely to affect multiple tissues and cell types in addition to our primary target (arterial endothelial cells). Indeed, anti-miR-712 treatment silenced miR-712 expression in multiple tissues, including whole blood and spleen (Supplementary Figure S14). Previously, miR-143/145 produced in endothelial cells were shown to be transferred to smooth muscle cells[46]. Consistent with this, miR-712 expression increased in media and adventitia of the LCA (Supplementary Figure S15). Moreover, we found that miR-712 expression was increased in blood following partial carotid ligation surgery, but not in sham controls and

anti-miR-712 treatment inhibited it (Supplementary Figure S5; S14a). We speculate that miR-712 produced in endothelial cells under *d-flow* conditions can be transferred to smooth muscle cells and blood, where it may have functional impact leading to robust atherosclerosis.

Since miR-712 is a murine-specific miRNA, its therapeutic value in human atherosclerosis could be limited. In this study, however, we identified miR-205 as a human homolog of the murine miR-712. It is unclear why our initial microarray study did not show statistically significant change in miR-205 expression in the LCA compared to RCA. One possibility is an inherent limitations in the miRNA array probe design[47]. However, using specific qPCR probes for precursor- and mature miR-205, we found that miR-205 is flow-sensitive, like miR-712, in endothelial cells both *in vitro* and *in vivo.* We also showed that miR-205 shares the same seed sequence with miR-712, and is highly conserved in most vertebrates including humans and mice (Figure 7a) and targets TIMP3. Therefore, knowledge gained from the miR-712 study could be translatable to humans, providing a potential clinical relevance.

In conclusion, we identified a mechanism by which mechanosensitive miR-712 can be generated from the pre-ribosomal RNA gene in a XRN1-dependent, but DGCR8-independent and DICER1-dependent manner, providing novel evidence that flow-sensitive miRNAs could be derived from an unexpected yet abundant source, pre-ribosomal RNAs. In addition, we demonstrate that anti-miRs targeting mechanosensitive miRNAs could be used to inhibit atherosclerosis. Our findings clearly demonstrate TIMP3 as a major target of miR-712 that controls endothelial inflammation and atherosclerosis. We propose that *d-flow* reduces the expression of XRN1, which increases miR-712 expression derived from the pre-ribosomal RNA (Figure 8). Increased miR-712 downregulates TIMP3 expression, which in turn, activates MMPs and ADAM proteases, leading to endothelial inflammation, hyperpermeability and arterial wall matrix fragmentation. miR-712 may also be transferred to blood and arterial medial layer where it may affect leukocytes and VSMC migration, respectively, resulting in multitude of pro-atherogenic changes (Figure 8). Targeting these mechanosensitive “athero-miRs” such as miR-712 and miR-205 may provide a new treatment paradigm in atherosclerosis.

Materials and Methods

Mouse partial carotid ligation surgery

All animal procedures were approved by the Animal Care and Use Committees at Emory University and University of California at Davis. Male C57BL/6 and *ApoE* $^{-/-}$ mice (Jackson Laboratory, Bar Harbor) were fed *ad libitum* with standard chow diet until surgery at 8 to 9 weeks of age. Mice were anesthetized with 3.5% isoflurane initially and then 1.5 to 2% during the entire procedure and underwent partial ligation[10]. The LCA bifurcation was exposed by blunt dissection and three of four caudal LCA branches (left external carotid, internal carotid, and occipital arteries) were ligated with 6-0 silk sutures, leaving the superior thyroid artery intact. The contralateral RCA was left intact as an internal control. Following surgery, analgesic buprenorphine (0.1 mg/kg) was administrated.

Two different models of atherosclerosis using ApoE$^{-/-}$ mice were used: the partial carotid ligation model fed a Paigen's high-fat diet (HFD; Science Diets) containing 1.25% cholesterol, 15% fat, and 0.5% cholic acid[1] and the Western diet-fed model for 3 months[31].

Ultrasonography

Following carotid ligation, *d-flow* in LCA was confirmed by Doppler ultrasonography (Vevo770, Visualsonics) with a 30-MHz probe. Briefly, mice were anaesthetized with 2% isoflurane and body temperature was monitored with a rectal probe and regulated by use of a heating pad. First, using B-mode, a long axis view of RCA and LCA was obtained. Thereafter, during diastole, a short-axis view was taken to visualize each artery[10, 48].

LNA-based anti-miR treatment or AdTIMP3 injection *in vivo*

Locked nucleic acid (LNA)-based miRNA inhibitor (anti-miR-712, Exiqon) were subcutaneously (s.c.) administered to 8-week-old male mice. For delivery efficiency testing, C57BL/6 mice (*n=3*) were subcutaneously administrated with 5 mg/kg of Texas-Red-615-labeled anti-miR-control (TEX615/ACGTCTATACGCCCA) or saline. After 24 hours, aortas were excised, and tissue samples were mounted on glass slides after counterstaining with 4′,6-diamidino-2-phenylindole (DAPI, Sigma). Samples were imaged using a Zeiss LSM 510 META confocal microscope (Carl Zeiss). To study the inhibition of miR-712, LNA-based anti-miR-712 (GTACCGCCCGGGTGAAGGA) or mismatched control was subcutaneously administered to C57BL/6 mice (*n=4*) one day before and on the day of partial ligation surgery. Animals were sacrificed on the 4 day post ligation and the carotid intimal RNAs were extracted and expression of miR-712 was determined by qPCR. For TIMP3 treatment, replication-defective recombinant adenoviruses encoding for TIMP3 (AdTIMP3) or empty vector control (AdRAD60) were used[49]. *ApoE*$^{-/-}$ mice were injected once with AdTIMP3 (10^8 pfu/animal, via tail vein) or control virus (AdRAD60, 10^8 pfu/animal) 5 days before partial carotid ligation and high fat diet for 2 weeks. For atherosclerosis studies, aortic trees were dissected out and processed for immunohistochemical analysis and plaque analysis was done using NIH Image J[10].

Synthesis of anti-miR712-DOTA

The conjugation of 5′-modified anti-miR-712 (5′-/5AmMC6/+CGCCCGGGTGAAGA-3′, Exiqon, and DOTA-NHS-ester (1,4,7,10-tetraazacyclododecane-1,4,7,10-tetraacetic acid mono (*N*-hydroxysuccinimide ester), Macrocyclics) followed a previously published paper[50] with modifications. 5′-modified anti-miR-712 (0.19 μmol, 1 mg) was suspended in 0.2 M borated buffer (0.3 mL, pH 8.5) and the dimethylsulfoxide solution (20 μL, Aldrich) of DOTA-NHS-ester (3.6 μmol, 2.8 mg) was added. After 5 hours of reaction, the mixture of DOTA conjugated anti-miR-712 was purified on Sephadex G-25 filled with double distilled water. Isolated anti-miR-712-DOTA was purified by HPLC with the following conditions: column Clarity Oligo-PR (250x10.00 mm, 5 micron, Phenomenex), gradient-solvent B (5–30%, 0–30 min, solvent A-0.1 M triethylammonium acetate (TEAA), solvent B-acetonitrile). Collected fractions were concentrated by centrifugation with an Amicon Ultra-4 centrifugal filter unit (MWCO: 3k). The concentrated solution was lyophilized and anti-miR-712-DOTA was stored at −20°C. MS analysis of sample was performed with

Thermo Fisher Scientific LTQ Orbitrap (San Jose, CA) operated in the centroid mode (Supplementary Figure S17). The deconvoluted mass from 1413.43 (Z=4) was detected at 5657.7 (Calc MW = 5657.6).

Radiolabeling of anti-miR-712-DOTA

$^{64}CuCl_2$ was obtained from Washington University Medical School under a protocol controlled by the University of California, Davis. $^{64}CuCl_2$ (3–5 mCi) was added into 0.1 M ammonium citrate buffer (0.1 mL, pH 5.5) and the anti-miR-712-DOTA (1 mM, 3–4 μL) in double distilled water was slowly added. After incubation for 1 hour at 40°C, the pH was adjusted to 7 by 1 M sodium hydroxide solution (trace metal, Aldrich). The reaction mixture was aspirated into 5 mL TEAA (10 mM, pH 7.0–7.5) in a 10 mL syringe. The solution was eluted through a Sep-Pak light C18 cartridge (Waters, Milford, MA). The C18 cartridge was eluted by 95% methanol (0.5–0.8 mL) to release the radiolabeled product. Concentrated solution was diluted with phosphate-buffered saline (PBS) to prepare a dose of ~0.2–0.3 mCi/150 μL. The specific activity of ^{64}Cu-anti-miR-712-DOTA was ~500–750 mCi/μmol. Radiochemical purity measured by a binary pump HPLC system (Waters), was more than 95% (Supplementary Figure S18).

Animal biodistribution and autoradiography studies

^{64}Cu-labeled anti-miR-712-DOTA was administered by tail vein injection of 2–3μg (0.2–0.3 mCi) in PBS (1x, 150 μL each animal). After 3 hours, animals were sacrificed by intraperitoneal injection of Euthasol (Western Medical Supply), blood and urine samples were collected, and the body was perfused with DMEM (Invitrogen) to remove blood and organs were collected. The aorta including the right and left carotid arteries were dissected and placed on a phosphor screen (Amersham Biosciences) for one hour. The phosphor screen was scanned on a Storm-860 imaging system (Amersham Biosciences) with 50 μm resolution. Radioactivity was counted with a 1470 automatic gamma counter (PerkinElmer). Tissue samples were weighed on a microbalance and the biodistribution is reported as percent injected radioactivity per gram (%ID/g) of tissue.

Serum Lipid Analysis

Serum lipid analysis was performed commercially (Cardiovascular Specialty Laboratories, Atlanta, GA) using a Beckman CX7 biochemical analyzer and reagents from Beckman Diagnostics (Fullerton, CA) for total cholesterol, triglycerides, HDL and LDL[51].

Plaque lesion analysis

Aorta and carotid arteries were isolated *en bloc* as described above from ligated ApoE$^{-/-}$ mice fed a high-fat diet for 2 weeks. RCA and LCA were photographed using a CCD camera (Moticam 2500, Motic) attached to a dissection microscope (EMZ-8TRD, MEIJI Techno) at 3x magnification and the opaque area covered by plaque and total artery area of LCA were quantified using NIH ImageJ software[1].

miRNA Microarray Procedures and Data Analysis

Intimal RNAs from three LCAs or RCAs were pooled to obtain ~30 ng total RNA[10]. miRNA microarray was performed using Illumina Mouse v2 MicroRNA expression BeadChip array (Illumina) at the Emory Biomarker Service Center[14]. After hybridization, BeadChips were scanned on the Illumina BeadArray Reader to determine probe fluorescence intensity and the raw probe intensities were normalized using the quantile normalization algorithm[1]. The normalized microarray data were statistically analyzed using Significance Analysis of *Microarrays software (SAM 3.0)*[1]. The differentially expressed miRNAs between LCA and RCA were identified for those that showed more than 1.5 fold-changes at less than 10% false discovery rate (FDR).

Quantitative real-time PCR (qPCR)

Total RNA was polyadenylated and reverse transcribed for use in a two-step qRT-PCR using the NCode miRNA First-Strand cDNA Synthesis and qRT-PCR kits (Invitrogen). The resulting cDNA was subjected to qPCR using the NCode universal reverse primer in conjunction with a sequence-specific forward primer for selected miRNAs. Small nucleolar RNA 202 (Sno202) and U6B were used as the internal control. using ABI StepOne Plus qPCR machine. The PCR conditions were 10 min at 95 °C, followed by 40 cycles of 95 °C for 4 s and 60 C for 30 s. For measurement of mRNA targets, qPCR was performed on selected genes using Brilliant II SYBR Green QPCR Master Mix (Stratagene) with custom designed primers using 18S as housekeeping control[1]. Fold changes between LCA and RCA were determined for all targets using the ΔΔCt method [1]. Sequences for primers used for miRNA expression and mRNA expression studies have been listed in Supplementary Table S3 and S4, respectively.

Mature and precursor miRNA assays were performed using MicroRNA quantification was performed by SYBR green qPCR assay using miScript reverse transcription kit (Qiagen) according to the manufacturer's instructions. qPCR was performed using miScript SYBR Green PCR kit (Qiagen) with miScript universal primer (U6B) and the miRNA-specific forward primers and relative fold change was calculated[1]. The specific mature and pre-miR primers were purchased from Qiagen. Other primer sequences used for microarray validation were designed based on the miRNA sequences obtained from the miRBase database (http://microrna.sanger.ac.uk/) (Supplementary Table S3). Each reaction was performed in duplicate with a final volume of 20 μl containing 2 μl of the cDNA, 10 μl of 2× SYBR Green PCR Master mix, of 2 μl and 10× miScript universal primer and 10× miScript primer assay. The amplification profile was denaturation at 95°C, 15 min, followed by 40 cycles of 94°C, 15 s; 55°C, 30 s, and 70°C, 30 s.

En face in situ hybridization

C57BL/6 mice were sacrificed by CO_2 inhalation and perfused first with saline containing heparin and then with formalin. Aortas were carefully excised, dissected free of surrounding fat tissue, fixed in 4% paraformaldehyde, and tissue samples from LCA and RCA as well as the greater and lesser curvature of the aortic arch taken. For, i*n situ* hybridization, *en face* samples were hybridized with 5′, 3′- Digoxigenin (DIG)-mmu-miR-712 detection probe (Exiqon) at 60°C for 18 h, followed by peroxidase-conjugated anti-DIG antibody (DIG-

POD, Roche). Signal amplification was done by tyramide signal amplification (TSA) using the Plus cyanine-3 system (TSA-Cy3, PerkinElmer)[52]. Samples were counterstained using DAPI (Sigma) and mounted on glass slides using fluorescence mounting medium (Dako). Samples were imaged using a Zeiss LSM 510 META confocal microscope (Carl Zeiss).

Integrated bioinformatics studies

We compared a list of putative miR-712 target genes generated by TargetScan[53] to the list of downregulated shear-sensitive genes[1]. The potential target genes were functionally annotated using DAVID[54] (http://david.abcc.ncifcrf.gov) and enriched onto the KEGG pathways[55] to generate a miR-712 interactome. Additional interactions among TIMP3 associated genes were identified through physical protein-protein interaction (PPI) (ftp://ftp.ncbi.nih.gov/gene/GeneRIF/), transcription factor-target relations (TF-target)[56] and enriched by adding non-mechanosensitive genes with known associations to *TIMP3* using iHOP[57].

Immunohistochemistry

Following treatment, ApoE$^{-/-}$ mice were euthanized and perfused with saline containing heparin as described above. LCA and RCA were collected *en bloc* along with the heart, aortic arch, trachea, esophagus, and surrounding fat tissue. Tissue was embedded in optimal cutting temperature (OCT) compound (Tissue-Tek), frozen on liquid nitrogen and stored at −80°C until used. Frozen sections were made starting from the level of the right subclavian artery bifurcation, 300 μm was trimmed away and three sets of ten consecutive 7 μm thick sections were taken at 300 μm intervals constituting the ‘proximal’ and ‘middle’ portions of the artery. To visualize atherosclerosis development, Oil red O staining was carried out using frozen sections using preheated Oil Red O stain at 60°C for 6 minutes. The slides were differentiated in 85% propylene glycol for 1 in and rinsed with 2 changes of distilled water and counterstaining was done using modified Mayer’s Hematoxylin for 1 min[10]. Sections were fixed in a 1:1 mixture of methanol/acetone for 10 min at RT and then blocked (1 h, at RT) using 10% (v/v) donkey serum in PBS. Immunohistochemical staining was carried out using following antibodies: versican fragment (1:300) (Abcam), TIMP3 (Abcam) (1:50), VE-cadherin (Santa Cruz) (1:50) and CD45-biotin (eBioscience) (1:100) overnight at 4°C. Secondary staining for CD45-biotin antibody was performed using streptavidin-conjugated rhodamine red X (RRX; Invitrogen) while DyLight 549-conjugated donkey anti-rabbit secondary antibody (Jackson Immunoresearch) (1:250) was used for versican and TIMP3. Samples were imaged using a Zeiss LSM 510 META confocal microscope (Carl Zeiss).

Cell culture and shear experiments

Immortalized mouse arterial endothelial cells (iMAEC) were generated from C57BL/6 mice. Briefly, aortas from 4-week-old male mice were dissected out and transferred (lumen side down) to a bead of collagen gel consisting of a mixture of type I collagen (Bio-Rad) and EGM2-MV (Lonza) to the final concentration of 1.75mg/ml and were left undisturbed. The explants were observed daily and cultured in incubator in 37°C and 5% CO_2. For cell immortalization, cells were incubated with 10^5 neomycin-resistant colony-forming units of the retrovirus vector N-TKmT in 1 mL of complete medium per well in the presence of 8

mg/mL polybrene (Sigma) (cushing AJP). The virus-containing medium was replaced 3 hours later with fresh complete medium and G418-resistant cells, were subcultured. All cells were maintained in 10% heat inactivated fetal bovine serum (FBS; Atlanta Biologicals), 100μM MEM Non-Essential Amino Acids, 1% Antibiotic-Antimycotic (GIBCO) containing Dulbecco's modified Eagle medium (DMEM, GIBCO) on 0.1% gelatin-coated 100-mm dishes at 37°C and 5% CO_2. For shear experiments, confluent iMAEC in 100-mm dishes were exposed to steady laminar (LS, 15 dyn/cm^2), oscillatory shear stress (OS, ±5 dyn/cm^2), or static conditions for 24 h using a cone-and-plate shear device for 24 hours[58]. Briefly, 100-mm cell culture dishes having confluent iMAEC cells were cultured under LS or OS, while plates at static condition served as controls.

Transient transfections with oligonucleotides

For the functional tests of miR-712 *in vitro*, cells were transiently transfected with anti-miR-712 (400nM; Exiqon), mismatched anti-miR control (400nM; Exiqon), pre-miR-712 (20nM; Ambion), or control-pre-miR (20nM; Ambion) using Oligofectamine (Invitrogen), following manufacturer's protocol as described previously[14]. Cells were sheared for 24 h after transfection.

Preparation of whole cell lysate and immunoblotting

Following treatment, cells were washed three times with ice-cold PBS and lysed with 600 μl of RIPA buffer. The protein content of each sample was determined by Bio-Rad DC assay. Aliquots of cell lysate were resolved by size on 10% SDS-polyacrylamide gels and subsequently transferred to a polyvinylidene difluoride membrane (Millipore). The membrane was incubated with following antibodies: TIMP3 (Abcam;1:1000), XRN1 (Abcam; 1:1000), DGCR8 (Sigma; 1:500), DICER1 (Sigma; 1:1000), overnight at 4°C, followed by secondary antibody (Bio-Rad; 1:5000) for 1 h at room temperature. Protein expression was detected by a chemiluminescence method. Full sized scans of all Western blots are provided in Supplementary Figure S19 and S20.

Isolation of endothelial RNA from mouse aortic arch

Aortic arch was harvested from C57BL/6 mice and opened *en face*. The endothelium was placed against a nitrocellulose-membrane soaked in isopropanol for 5 minutes, and the media and adventitia were peeled away leaving the endothelial monolayer adherent to the nitrocellulose membrane and RNA was extracted using Qiagen miREasy kit. For each experiment, LC and GC regions from two to four mice were pooled. A panel of markers genes for endothelium (PECAM1), smooth muscle (αSMA) and immune cell (CD11b) was used to determine the enrichment of endothelial RNA from the preparation.

Dual-luciferase activity assays

Measurement of firefly luciferase activity was obtained at room temperature using Luc-Pair miR Luciferase Assay Kit (GeneCopoeia) and a single tube luminometer (Model TD 20/20 Turner Designs, Sunnyvale, CA). Dual-luciferase reporter constructs containing 3′UTR of TIMP3 with miR-712 binding sites (GAAGGAA) (GeneCopoeia) or 3′UTR of TIMP3 with mutated miR-712-binding site (GTTGGAA) (custom cloned at Emory Molecular Biology

core facility) were transfected into iMAECs using a *Nucleofection* Kit (*Lonza)*. iMAECs were transfected first with wild-type or mutated target gene 3′-UTR using *HUVEC Nucleofector*™ Kit (*Lonza*) and were allowed to recover for 24 h. Second transfection was performed using increasing concentrations pre-miR-712 and LNA-anti-miR-712 or respective mismatch controls with Oligofectamine 2000 (Invitrogen). Firefly and Renilla luciferase activities were measured using a Luc-Pair™ miR Luciferase Assay (GeneCopoeia) as per manufacturer's recommendations.

Smooth muscle cell proliferation and migration

Following anti-miR-712 transfections for 24 h, murine VSMCs were placed in serum-free medium and stimulated with 10 ng/mL of PDGF-BB for 24 h and cell proliferation was determined by WST1 assay[59]. To determine migration, VSMCs were transfected with anti-miR-712 or control and were maintained in serum-free media overnight before migration assay. VSMCs were added at a density of 5×10^4 cells/well to the upper chamber of a Transwell dish coated with type I rat tail collagen (BD Bioscience)[59]. VSMCs were stimulated with PDGF-BB (10 ng/mL) in the lower chamber. After 4 hours, migrated cells were fixed, stained with DAPI and counted from five random fields.

Northern Blotting

Total RNAs were obtained from iMAECs and 25μg/lane were electrophoresed on 12% denaturating urea gel and transferred on to nitrocellulose membrane. DIG-labeled miR-712 probe (IDT) was used for Northern blotting. Anti-DIG antibody conjugated to alkaline phosphatase was used for chemiluminescent detection[60]. 5S rRNA was used as loading control.

Monocyte Adhesion Assay

iMAECs were transfected with pre-miR-712 or control for 24 h and post transfection, leukocyte adhesion assay was performed using 2.5 X 10^5 fluorescent-labeled J774.4 mouse monocyte cells. Adherent cells were quantified by fluorescence microscopy[14].

EC permeability (*in vitro* and *in vivo*)

Cultrex® *In vitro* Angiogenesis Assay Endothelial Cell Invasion Kit was used to determine endothelial permeability using Transfected iMAECs according to manufacturer's protocol. Fluorescence signals from FITC-dextran in the lower chamber were quantified and plotted as arbitrary fluorescence units. For *in vivo* endothelial permeability assay, 1% Evans Blue dye (Sigma) was injected via tail vein (100 μl/animal) one week after partial ligation surgery. Animals were sacrificed after 30 min, aortic trees were isolated and imaged by bright field microscopy. Evans Blue leakage into the carotids was quantified by NIH Image J software.

Soluble-TNFα ELISA

iMAECs treated with TIMP3 expression vector, TIMP3 siRNA, pre-miR-712, anti-miR-712, and their respective controls for 24 h, and then exposed to static or shear conditions for 24 h.

s-TNFα in conditioned media was measured using mouse soluble-TNFα ELISA kit (R&D Biosystems) following the manufacturer's protocol.

Statistical analyses

Statistical analyses were carried out with Graph-Pad Prism (GraphPad Software). All error bars reported are SEM unless otherwise indicated. Pairwise comparisons were performed using one-way Student *t*-tests. Multiple comparisons of means were performed using 1-way ANOVA followed by Tukey's multiple comparison tests. Differences between groups were considered significant at P values below 0.05. All miRNA array data were analyzed with GenomeStudio software (Illumina).

Supplementary Material

Refer to Web version on PubMed Central for supplementary material.

Acknowledgments

This work was supported by funding from NIH grants HL095070, HL70531and a World Class University Project (R31-2008-000-10010-0) from the Ministry of Science, Technology and Education of S. Korea (MEST) to HJ, HHSN268201000043C to HJ and KF, and by the Global Frontier Project grant (NRF-M1AXA-002-2010-0029763) and the grant (2011-0014992) from MEST to WK. SK is an American Heart Association postdoctoral fellow. We thank Dr. Oskar Laur at the Emory Custom Cloning Core facility for generating TIMP3 mutants.

References

1. Ni CW, et al. Discovery of novel mechanosensitive genes in vivo using mouse carotid artery endothelium exposed to disturbed flow. Blood. 2010; 116:e66–73. [PubMed: 20551377]
2. Berk BC. Atheroprotective signaling mechanisms activated by steady laminar flow in endothelial cells. Circulation. 2008; 117:1082–1089. [PubMed: 18299513]
3. Ku DN, Giddens DP, Zarins CK, Glagov S. Pulsatile Flow and Atherosclerosis in the Human Carotid Bifurcation - Positive Correlation between Plaque Location and Low and Oscillating Shear-Stress. Arteriosclerosis. 1985; 5:293–302. [PubMed: 3994585]
4. McCormick SM, et al. DNA microarray reveals changes in gene expression of shear stressed human umbilical vein endothelial cells. Proc Natl Acad Sci U S A. 2001; 98:8955–8960. [PubMed: 11481467]
5. Chiu JJ, Chien S. Effects of disturbed flow on vascular endothelium: pathophysiological basis and clinical perspectives. Physiol Rev. 2011; 91:327–387. [PubMed: 21248169]
6. Davies PF. Hemodynamic shear stress and the endothelium in cardiovascular pathophysiology. Nat Clin Pract Cardiovasc Med. 2009; 6:16–26. [PubMed: 19029993]
7. Tzima E, et al. A mechanosensory complex that mediates the endothelial cell response to fluid shear stress. Nature. 2005; 437:426–431. [PubMed: 16163360]
8. Passerini AG, et al. Coexisting proinflammatory and antioxidative endothelial transcription profiles in a disturbed flow region of the adult porcine aorta. Proc Natl Acad Sci U S A. 2004; 101:2482–2487. [PubMed: 14983035]
9. Dai G, et al. Distinct endothelial phenotypes evoked by arterial waveforms derived from atherosclerosis-susceptible and -resistant regions of human vasculature. Proc Natl Acad Sci U S A. 2004; 101:14871–14876. [PubMed: 15466704]
10. Nam D, et al. Partial carotid ligation is a model of acutely induced disturbed flow, leading to rapid endothelial dysfunction and atherosclerosis. Am J Physiol Heart Circ Physiol. 2009; 297:H1535–1543. [PubMed: 19684185]

11. Magid R, Murphy TJ, Galis ZS. Expression of matrix metalloproteinase-9 in endothelial cells is differentially regulated by shear stress. Role of c-Myc. J Biol Chem. 2003; 278:32994–32999. [PubMed: 12816956]
12. Chatzizisis YS, Coskun AU, Jonas M, Edelman ER, Feldman CL, Stone PH. Role of endothelial shear stress in the natural history of coronary atherosclerosis and vascular remodeling: molecular, cellular, and vascular behavior. J Am Coll Cardiol. 2007; 49:2379–2393. [PubMed: 17599600]
13. Arroyo AG, Iruela-Arispe ML. Extracellular matrix, inflammation, and the angiogenic response. Cardiovasc Res. 2010; 86:226–235. [PubMed: 20154066]
14. Ni CW, Qiu H, Jo H. MicroRNA-663 upregulated by oscillatory shear stress plays a role in inflammatory response of endothelial cells. Am J Physiol Heart Circ Physiol. 2011; 300:H1762–1769. [PubMed: 21378144]
15. Gregory RI, et al. The Microprocessor complex mediates the genesis of microRNAs. Nature. 2004; 432:235–240. [PubMed: 15531877]
16. Lee Y, et al. The nuclear RNase III Drosha initiates microRNA processing. Nature. 2003; 425:415–419. [PubMed: 14508493]
17. Denli AM, Tops BB, Plasterk RH, Ketting RF, Hannon GJ. Processing of primary microRNAs by the Microprocessor complex. Nature. 2004; 432:231–235. [PubMed: 15531879]
18. Berezikov E, Chung WJ, Willis J, Cuppen E, Lai EC. Mammalian mirtron genes. Mol Cell. 2007; 28:328–336. [PubMed: 17964270]
19. Ruby JG, Jan CH, Bartel DP. Intronic microRNA precursors that bypass Drosha processing. Nature. 2007; 448:83–86. [PubMed: 17589500]
20. Geerlings TH, Vos JC, Raue HA. The final step in the formation of 25S rRNA in Saccharomyces cerevisiae is performed by 5′-->3′ exonucleases. RNA. 2000; 6:1698–1703. [PubMed: 11142370]
21. Wu Y, Wei B, Liu H, Li T, Rayner S. MiRPara: a SVM-based software tool for prediction of most probable microRNA coding regions in genome scale sequences. BMC Bioinformatics. 2011; 12:107. [PubMed: 21504621]
22. Ritchie W, Theodule FX, Gautheret D. Mireval: a web tool for simple microRNA prediction in genome sequences. Bioinformatics. 2008; 24:1394–1396. [PubMed: 18453555]
23. Black RA. TIMP3 checks inflammation. Nat Genet. 2004; 36:934–935. [PubMed: 15340428]
24. George SJ, Wan S, Hu J, MacDonald R, Johnson JL, Baker AH. Sustained reduction of vein graft neointima formation by ex vivo TIMP-3 gene therapy. Circulation. 2011; 124:S135–142. [PubMed: 21911803]
25. Federici M, et al. Timp3 deficiency in insulin receptor-haploinsufficient mice promotes diabetes and vascular inflammation via increased TNF-alpha. J Clin Invest. 2005; 115:3494–3505. [PubMed: 16294222]
26. Karangelis DE, et al. Glycosaminoglycans as key molecules in atherosclerosis: the role of versican and hyaluronan. Curr Med Chem. 2010; 17:4018–4026. [PubMed: 20939824]
27. Jonsson-Rylander AC, et al. Role of ADAMTS-1 in atherosclerosis: remodeling of carotid artery, immunohistochemistry, and proteolysis of versican. Arterioscler Thromb Vasc Biol. 2005; 25:180–185. [PubMed: 15539621]
28. Casagrande V, et al. Overexpression of tissue inhibitor of metalloproteinase 3 in macrophages reduces atherosclerosis in low-density lipoprotein receptor knockout mice. Arterioscler Thromb Vasc Biol. 2012; 32:74–81. [PubMed: 22015660]
29. Lei M, Kleinstreuer C, Truskey GA. A focal stress gradient-dependent mass transfer mechanism for atherogenesis in branching arteries. Med Eng Phys. 1996; 18:326–332. [PubMed: 8963477]
30. Herrmann RA, Malinauskas RA, Truskey GA. Characterization of sites with elevated LDL permeability at intercostal, celiac, and iliac branches of the normal rabbit aorta. Arterioscler Thromb. 1994; 14:313–323. [PubMed: 8305425]
31. Park JG, et al. Peroxiredoxin 2 deficiency exacerbates atherosclerosis in apolipoprotein E-deficient mice. Circ Res. 2011; 109:739–749. [PubMed: 21835911]
32. Schultz J, Wolf M. ITS2 sequence-structure analysis in phylogenetics: a how-to manual for molecular systematics. Mol Phylogenet Evol. 2009; 52:520–523. [PubMed: 19489124]

33. Moy TI, Silver PA. Nuclear export of the small ribosomal subunit requires the ran-GTPase cycle and certain nucleoporins. Genes Dev. 1999; 13:2118–2133. [PubMed: 10465789]
34. Cardellini M, et al. TIMP3 is reduced in atherosclerotic plaques from subjects with type 2 diabetes and increased by SirT1. Diabetes. 2009; 58:2396–2401. [PubMed: 19581416]
35. Wight TN, Merrilees MJ. Proteoglycans in Atherosclerosis and Restenosis: Key Roles for Versican. Circulation Research. 2004; 94:1158–1167. [PubMed: 15142969]
36. Ponnuchamy B, Khalil RA. Role of ADAMs in Endothelial Cell Permeability: Cadherin Shedding and Leukocyte Rolling. Circulation Research. 2008; 102:1139–1142. [PubMed: 18497310]
37. Chen K, Fan W, Wang X, Ke X, Wu G, Hu C. MicroRNA-101 mediates the suppressive effect of laminar shear stress on mTOR expression in vascular endothelial cells. Biochem Biophys Res Commun. 2012; 427:138–142. [PubMed: 22989749]
38. Wang KC, et al. Role of microRNA-23b in flow-regulation of Rb phosphorylation and endothelial cell growth. Proc Natl Acad Sci U S A. 2010; 107:3234–3239. [PubMed: 20133741]
39. Qin X, et al. MicroRNA-19a mediates the suppressive effect of laminar flow on cyclin D1 expression in human umbilical vein endothelial cells. Proceedings of the National Academy of Sciences. 2010; 107:3240–3244.
40. Weber M, Baker MB, Moore JP, Searles CD. MiR-21 is induced in endothelial cells by shear stress and modulates apoptosis and eNOS activity. Biochemical and Biophysical Research Communications. 2010; 393:643–648. [PubMed: 20153722]
41. Fang Y, Shi C, Manduchi E, Civelek M, Davies PF. MicroRNA-10a regulation of proinflammatory phenotype in athero-susceptible endothelium in vivo and in vitro. Proceedings of the National Academy of Sciences. 2010; 107:13450–13455.
42. Marin T, et al. Mechanosensitive microRNAs-role in endothelial responses to shear stress and redox state. Free Radic Biol Med. 2013; 64:61–68. [PubMed: 23727269]
43. Zhou J, et al. MicroRNA-21 targets peroxisome proliferators-activated receptor-α in an autoregulatory loop to modulate flow-induced endothelial inflammation. Proceedings of the National Academy of Sciences. 2011; 108:10355–10360.
44. Wu W, et al. Flow-Dependent Regulation of Krüppel-Like Factor 2 Is Mediated by MicroRNA-92a. Circulation. 2011; 124:633–641. [PubMed: 21768538]
45. Wei Y, Nazari-Jahantigh M, Neth P, Weber C, Schober A. MicroRNA-126, -145, and -155: a therapeutic triad in atherosclerosis? Arterioscler Thromb Vasc Biol. 2013; 33:449–454. [PubMed: 23324496]
46. Hergenreider E, et al. Atheroprotective communication between endothelial cells and smooth muscle cells through miRNAs. Nat Cell Biol. 2012; 14:249–256. [PubMed: 22327366]
47. Pritchard CC, Cheng HH, Tewari M. MicroRNA profiling: approaches and considerations. Nat Rev Genet. 2012; 13:358–369. [PubMed: 22510765]
48. Nam D, et al. A model of disturbed flow-induced atherosclerosis in mouse carotid artery by partial ligation and a simple method of RNA isolation from carotid endothelium. J Vis Exp. 2010
49. Baker AH, Zaltsman AB, George SJ, Newby AC. Divergent effects of tissue inhibitor of metalloproteinase-1, -2, or -3 overexpression on rat vascular smooth muscle cell invasion, proliferation, and death in vitro. TIMP-3 promotes apoptosis. J Clin Invest. 1998; 101:1478–1487. [PubMed: 9502791]
50. Hnatowich DJ, et al. Comparative properties of a technetium-99m-labeled single-stranded natural DNA and a phosphorothioate derivative in vitro and in mice. J Pharmacol Exp Ther. 1996; 276:326–334. [PubMed: 8558450]
51. Li L, Chen W, Rezvan A, Jo H, Harrison DG. Tetrahydrobiopterin Deficiency and Nitric Oxide Synthase Uncoupling Contribute to Atherosclerosis Induced by Disturbed Flow. Arterioscler Thromb Vasc Biol. 2011
52. Obernosterer G, Martinez J, Alenius M. Locked nucleic acid-based in situ detection of microRNAs in mouse tissue sections. Nat Protoc. 2007; 2:1508–1514. [PubMed: 17571058]
53. Lewis BP, Shih IH, Jones-Rhoades MW, Bartel DP, Burge CB. Prediction of mammalian microRNA targets. Cell. 2003; 115:787–798. [PubMed: 14697198]
54. Dennis G Jr, et al. DAVID: Database for Annotation, Visualization, and Integrated Discovery. Genome Biol. 2003; 4:P3. [PubMed: 12734009]

55. Kanehisa M, Goto S. KEGG: kyoto encyclopedia of genes and genomes. Nucleic Acids Res. 2000; 28:27–30. [PubMed: 10592173]

56. Wingender E. The TRANSFAC project as an example of framework technology that supports the analysis of genomic regulation. Brief Bioinform. 2008; 9:326–332. [PubMed: 18436575]

57. Fernandez JM, Hoffmann R, Valencia A. iHOP web services. Nucleic Acids Res. 2007; 35:W21–26. [PubMed: 17485473]

58. Sorescu GP, et al. Bone morphogenic protein 4 produced in endothelial cells by oscillatory shear stress stimulates an inflammatory response. J Biol Chem. 2003; 278:31128–31135. [PubMed: 12766166]

59. Williams HC, et al. Role of coronin 1B in PDGF-induced migration of vascular smooth muscle cells. Circ Res. 2012; 111:56–65. [PubMed: 22619279]

60. Varallyay E, Burgyan J, Havelda Z. MicroRNA detection by northern blotting using locked nucleic acid probes. Nat Protoc. 2008; 3:190–196. [PubMed: 18274520]

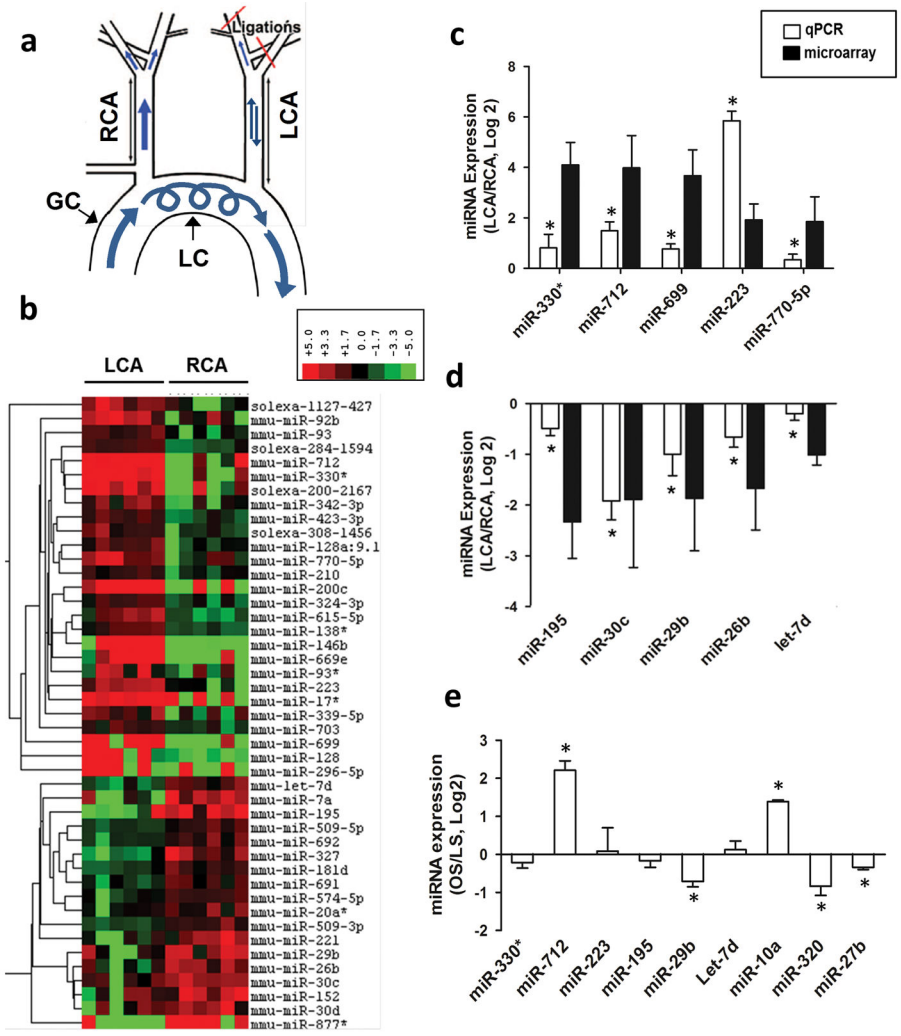

Figure 1. miR-712 is a flow-sensitive microRNA upregulated by *d-flow in vitro* and *in vivo*

(a) The schema shows naturally occurring *d-flow* (lesser curvature, LC) and stable flow (*s-flow)* regions (greater curvature, GC) in the aortic arch. Also shown is the surgically induced *d-flow* in partial carotid ligation model in which three of the four caudal branches of the left common carotid artery (LCA) are ligated, while the contralateral right common carotid artery (RCA) remains untouched as an internal control. (b) Endothelial-enriched total RNAs obtained from intima of mouse (C57BL/6) left carotid (flow-disturbed LCA) and right carotid (contralateral control, RCA) at 48 h post-ligation, were analyzed by gene array (Illumina BeadChip). Hierarchical clustering analyses of mechanosensitive miRNAs found in LCA endothelium compared to that of RCA are shown as heat maps. The color represents the expression level of the gene. Red represents high expression, while green represents low expression. The expression levels are continuously mapped on the color scale provided at the top of the figure. Each column represents a single sample pooled from 3 different LCAs or RCAs, and each row represents a single miRNA probe (n=3). (c–f) **Validation of miRNA microarray results by qPCR** Quantitative PCR (qPCR), using additional independent RNA samples, was used to validate the above miRNA array data. Ten miRNAs

(5 up-, 5 down-regulated miRNAs at 48 hours post-ligation) were selected based on fold-change by flow. The qPCR study validated the microarray results for **(c)** 5 up-regulated (miR-712, -330*, -699, -223, and 770–5p) and **(d)** 5 down-regulated (miR-195, -30c, -29b, -26b and let-7d) miRNAs at the 48 h time point (n=5 each, data shown as mean ± s.e.m; * $p<0.05$ as determined by paired *t*-test). To further validate whether the mechanosensitive genes that were identified *in vivo* responded specifically to shear stress, we tested expression of these miRNAs *in vitro* using immortalized mouse aortic endothelial cells (iMAECs) that were subjected to laminar (LS) or oscillatory stress (OS), mimicking *s-flow* and *d-flow in vivo*, respectively [14]. Among the 9 different miRNAs examined, 7 miRNAs were differentially expressed under oscillatory shear (n=6 each, data shown as mean ± s.e.m; * $p<0.05$ as determined by paired *t*-test) **(e)**. These results showed that miR-712 was the most consistently and robustly upregulated miRNA both *in vivo* and under flow conditions *in vitro.*

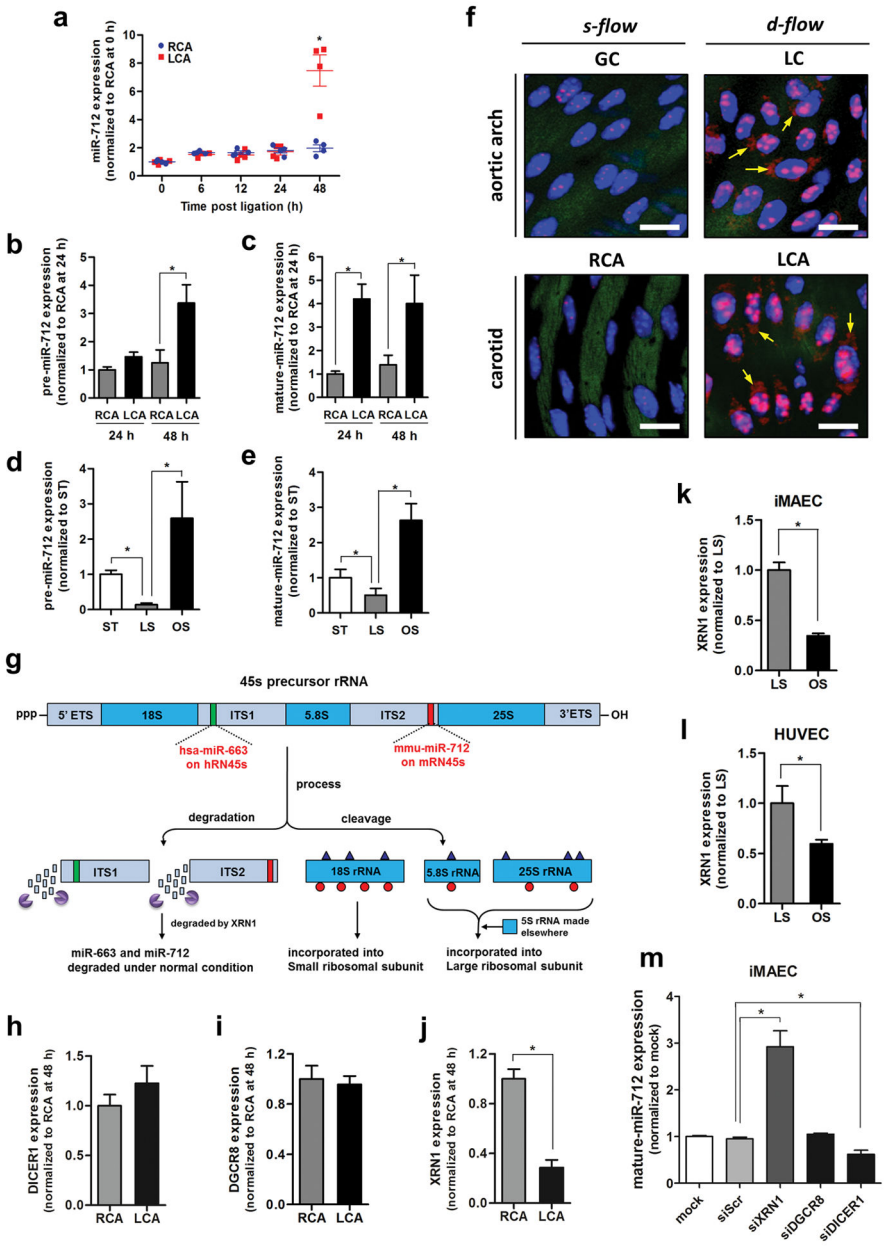

Figure 2. miR-712 is atypically derived from RN45S gene in XRN-1-dependent manner

(a) Expression of miR-712 was determined by qPCR using endothelial-enriched RNA obtained from LCA and RCA following partial carotid ligation in C57Bl6 mouse (0–48h) (n=4, data shown as mean ± s.e.m; * $p<0.05$ as determined by paired *t*-test). (b, c) Expression of pre-miR-712 and mature miR-712 by *d-flow* in LCA and RCA endothelium following partial ligation at 24 and 48 hours as above in (b) was quantitated by miScript miRNA qPCR assay (*n=8* each; *$p<0.05$ as determined by Student's *t*-test). (d, e) Expression of pre-miR-712 and mature miR-712 was measured by miScript miRNA qPCR in immortalized mouse aortic endothelial cells (iMAECs) exposed to laminar (LS), oscillatory shear (OS) or static (ST) for 24 h (n=6, data shown as mean ± s.e.m; * $p<0.05$ as determined by Student's *t*-test). (f) Aortic arch (LC and GC) and LCA and RCA obtained at

2-days post ligation obtained from control C57Bl6 mice were subjected to fluorescence *in situ* hybridization using digoxigenin-labeled miR-712 probe and anti-digoxigenin antibody, which was detected by tyramide signal amplification method using Cy-3 and confocal microscopy (shown in red), (n=6). Blue: DAPI nuclear stain; Green: auto-fluorescent elastic lamina; Arrows indicate cytosolic miR-712 expression. White scale bars = 20 μm. (g) shows the potential structure and processing of pre-ribosomal RNA gene, RN45s, which is composed of 18S, 5.8S and 28S rRNA sequences with 2 intervening spacers ITS1 and ITS2. The sequences matching murine miR-712 in ITS2 and its putative human counterpart miR-663 in ITS1 are indicated as well. (h–j) Expression of *DICER*, *DGCR8* and *XRN1* in mouse RCA and LCA (2-day post ligation) were determined by qPCR (n=4, data shown as mean ± s.e.m; * $p<0.05$ as determined by paired *t*-test). (k, l) *XRN1* expression in iMAECs and HUVECs exposed to LS or OS for 24 h was determined by qPCR (n=3 each, data shown as mean ± s.e.m; * $p<0.05$ as determined by Student's *t*-test). (m) miR-712 expression was induced by treating iMAECs with XRN1 siRNA but not by DGCR8 siRNA and DICER1 siRNA (n=3 each, data shown as mean ± s.e.m; * $p<0.05$ as determined by Student's *t*-test).

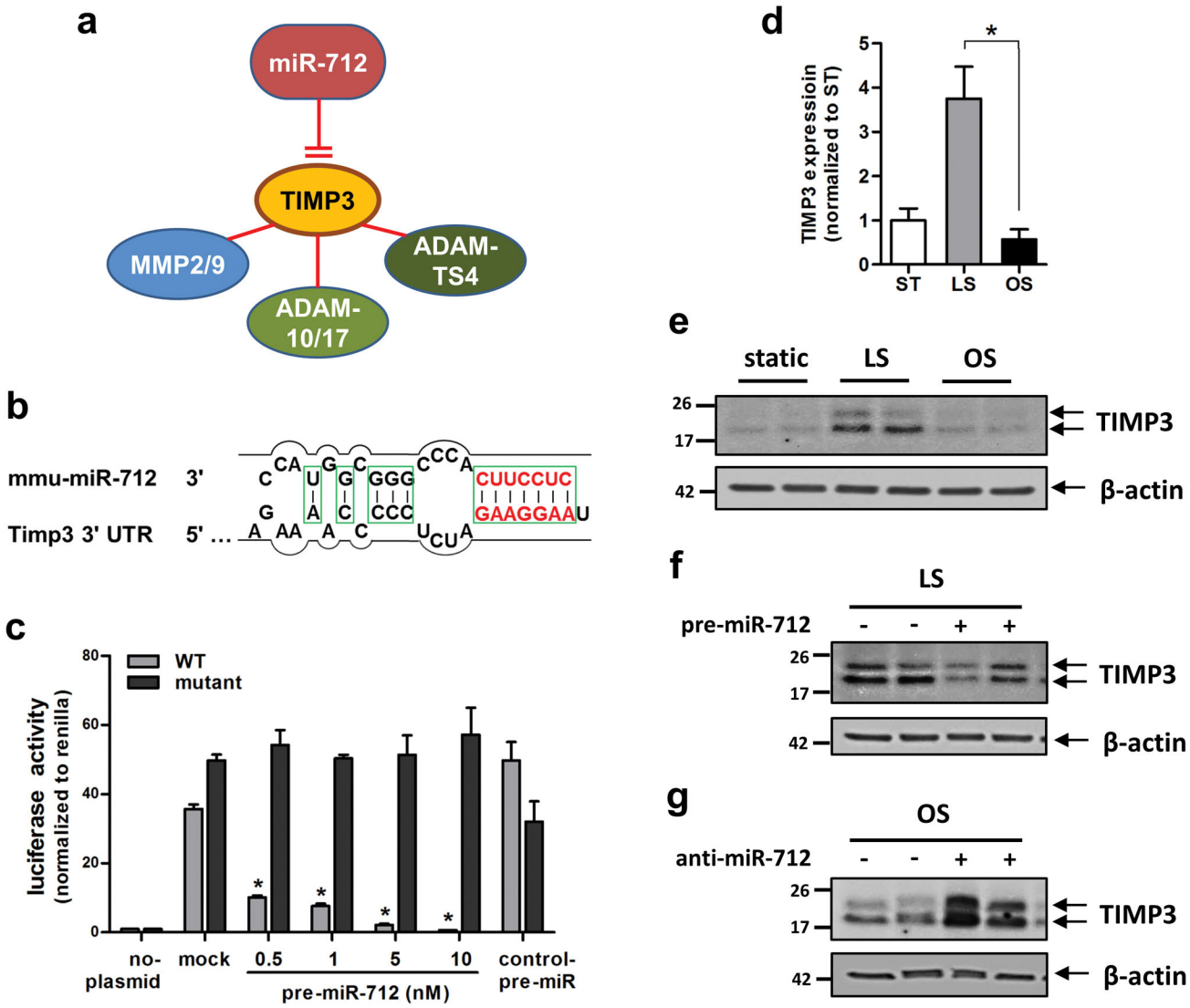

Figure 3. TIMP3 is the direct target of miR-712

(a) shows TIMP3 as a potential target of miR-712 and its link to putative downstream metalloproteinase targets. (b) shows the seed sequence of miR-712 and complementary 3′-UTR sequence of TIMP3. (c) iMAECs transfected with dual-luciferase reporter plasmids containing wild-type (WT) or mutant TIMP3-3′UTR, were treated with pre-miR-712 or control pre-miR. Firefly luciferase activity (normalized to control *Renilla* luciferase) indicating TIMP3 expression was determined using Luc-Pair miR Luciferase Assay Kit (n=3 each, data shown as mean ± s.e.m; * $p<0.05$ as determined by Student's *t*-test). (d) *TIMP3* expression in iMAECs determined by qPCR was decreased by exposure to OS compared to LS or ST for 24 h (n=6, data shown as mean ± s.e.m; * $p<0.05$ as determined by Student's *t*-test). (e–g) Representative Western blots show modulation of TIMP3 expression by treatment with shear stress in the presence of pre-miR-712 or anti-miR-712 for 24 h in iMAECs. (e) TIMP3 expression decreased by OS compared to LS for 24 h. (f) Treatment with pre-miR-712 (20 nM) down-regulated TIMP3 expression under LS condition. (g) anti-miR-712 (400 nM) treatment rescued OS-induced loss of TIMP3. β-actin was used as

internal loading control. Full sized scans of all Western blots are provided in Supplementary Figure S22.

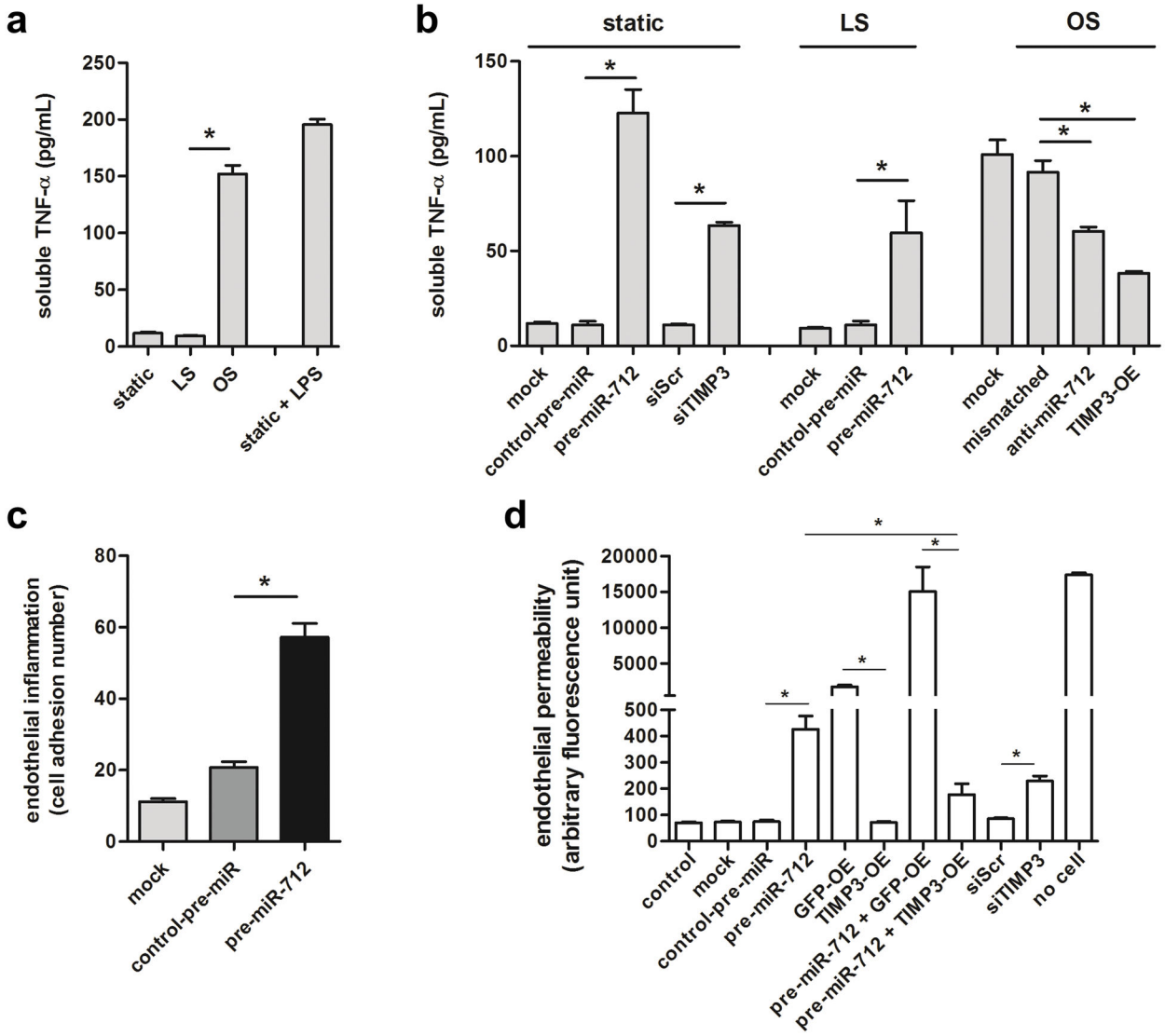

Figure 4. miR-712 induces endothelial inflammation and hyperpermeability changes

(a) iMAECs were exposed to static, LS, or OS for 24 h, and the conditioned media were used for TNFα ELISA. LPS was used as a positive control. (b) iMAECs were transfected with TIMP3 expression vector (TIMP3-OE), TIMP3 siRNA (150nM), pre-miR-712 (20nM), anti-miR-712 (400nM), and respective controls for 24 h. Cells were then exposed to static, LS or OS for 24 h, and s-TNFα in conditioned media was determined by ELISA. (n=6, data shown as mean ± s.e.m; * $p<0.05$ as determined by 1-way ANOVA). (c) iMAECs were transfected with pre-miR-712 (20nM) or control and leukocyte adhesion assay was performed using 2.5 X 10^5 fluorescent-labeled J774.4 mouse monocyte cells. Adherent cells were counted (n=5 independent experiments, data shown as mean ± s.e.m; * $p<0.05$ as determined by 1-way ANOVA). **(d)** iMAECs were transfected with TIMP3-OE or its GFP vector control (GFP-OE), TIMP3 or scrambled control siRNA (siTIMP3 or siScr, 150nM), pre-miR-712 or control-pre-miR (20nM), pre-miR-712 with GFP-OE or TIMP3-OE, and no treatment (control), transfection (mock) or no cell controls for 24 h. Cells were then exposed

to static, LS or OS for 24 h, and endothelial permeability was determined using a FITC-dextran based *in vitro* vascular permeability kit (Cultrex). Fluorescence signals from FITC-dextran in the lower chamber were quantified and plotted as arbitrary fluorescence units (n=3 each from two independent experiments, data shown as mean ± s.e.m; * $p<0.05$ as determined by 1-way ANOVA).

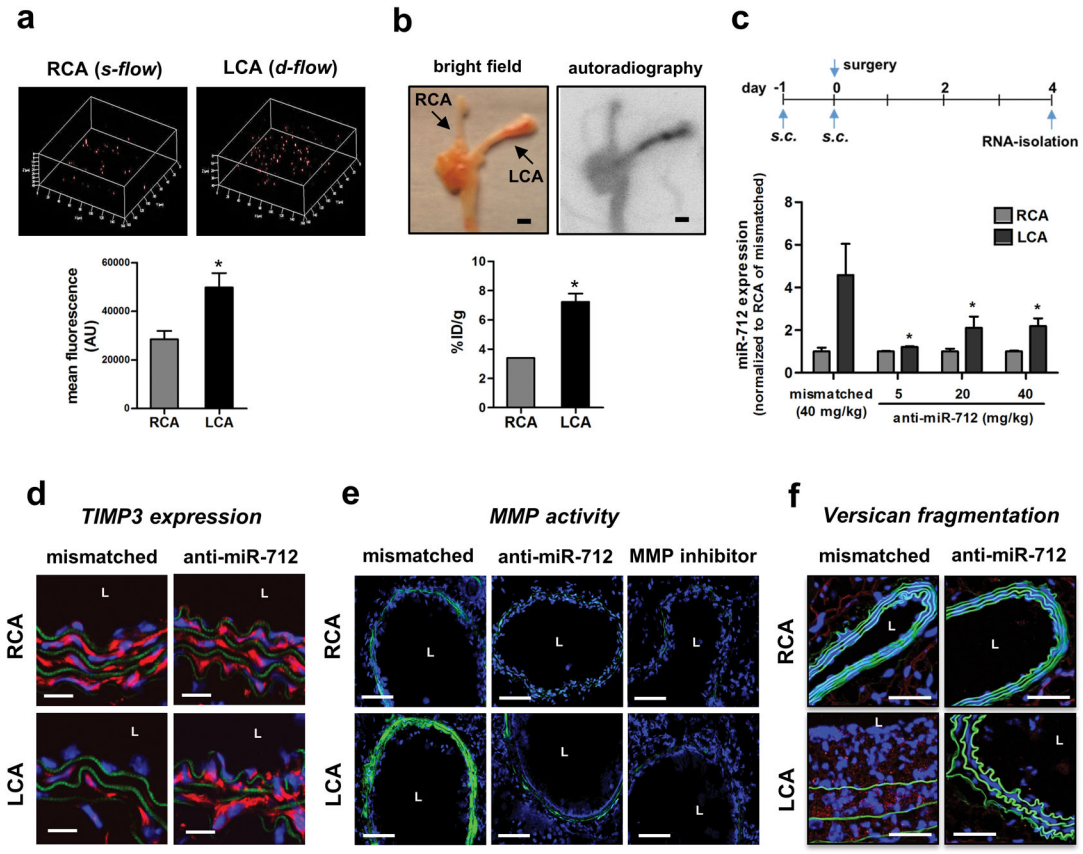

Figure 5. Anti-miR-712 silences miR-712 and restores TIMP3 expression *in vivo*

(a) TexRed-615-labeled control anti-miR or saline was injected (*s.c.*) in C57Bl6 mice. Carotid arteries were dissected out 24 h later, and using Zeiss 510 confocal microscope z-stack images of the en face sections were obtained. Images were rendered to 3D, bounding box was drawn on the area of interest and scaled cordinate axes were drawn and fluorescence signals from Red channel were processed and quantified. Graph shows mean fluorescence intensity of TexRed-615 signals from carotids (n=5, data shown as mean ± s.e.m) (b) Following partial carotid ligation and high-fat diet for 2 weeks, ApoE$^{-/-}$ mice were injected with ^{64}Cu-labelled anti-miR-712 via tail-vein. After 3 hours, aortic trees including carotids were prepared and autoradiographed, which was used to quantitate percentage of injected dose per gram (%ID/g) (n=6, data shown as mean ± s.e.m; * $p<0.05$ as determined by Student's *t*-test). Scale bar=1 mm. (c) To determine the optimal dose of anti-miR-712, C57Bl6 mice were injected with anti-miR-712 daily for 2 days (*s.c.* at 5, 20 or 40 mg/kg/day dose) and followed by partial carotid ligation. Mismatched anti-miR-712 (40 mg/kg/day) was used as a control. Endothelial-enriched RNAs were prepared from LCA and RCA obtained at 4-days post ligation, and miR-712 expression was determined by qPCR showing optimal effect at 5 mg/kg dose (n=4 each, data shown as mean ± s.e.m; * $p<0.05$ as determined by paired *t*-test). (d–f) ApoE$^{-/-}$ mice were partially ligated and fed high-fat diet for 1 week (d and e) or 2 weeks (f). RCA and LCA frozen sections obtained from these mice were used for immunofluorescence staining with antibody specific to TIMP3 shown in red Scale bar =20μm. (d) or versican fragment peptide DPEAAE shown in red. Scale bar

=20μm. (f), and *in situ* zymography using DQ-gelatin (green) to determine MMP activity (e). As a control for the MMP activity assay, some LCA and RCA sections were incubated with MMP inhibitor 1. Blue: DAPI and green: autofluorescent elastic lamina (L= lumen of the artery). Scale bar =50μm.

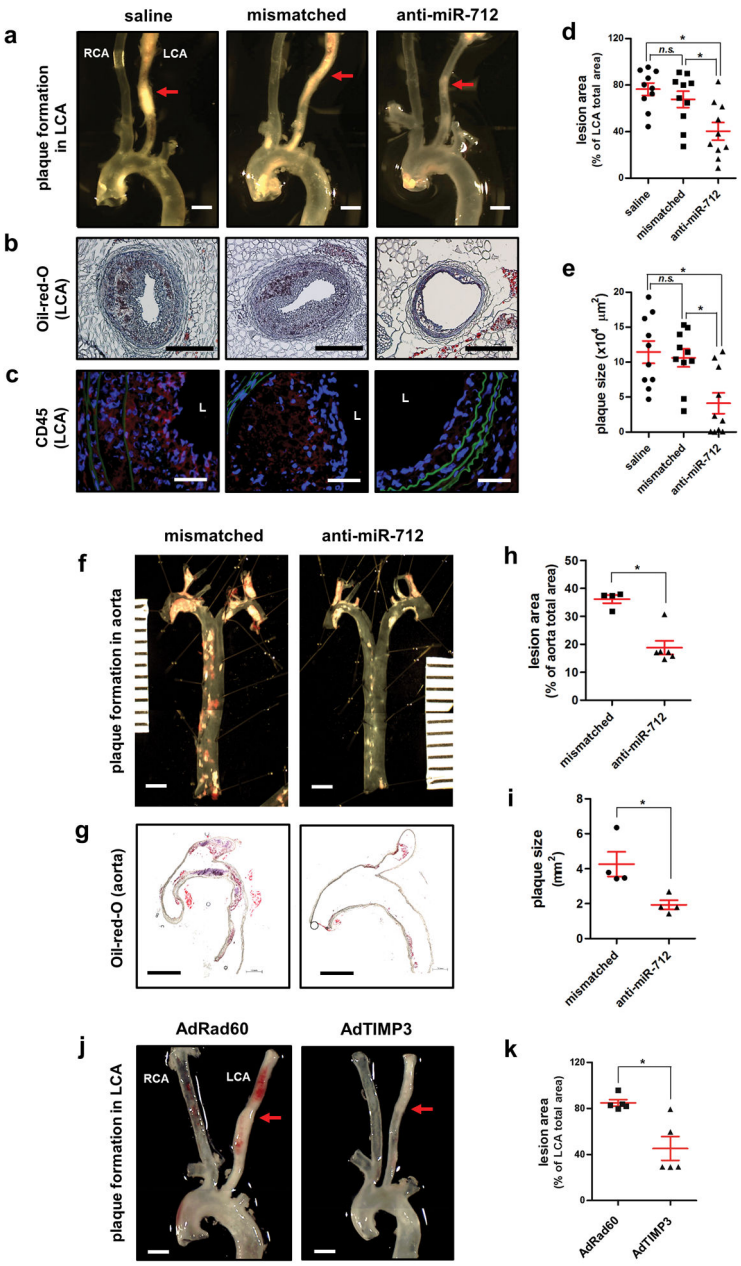

Figure 6. Anti-miR-712 or adenoviral TIMP3 reduces atherosclerosis in ApoE$^{-/-}$ mice

For acute study, *ApoE*$^{-/-}$ mice were pretreated twice with anti-miR-712 or mismatched control (5mg/kg each, *s.c.*) or saline on 1 and 2 days prior to partial ligation. Mice were then fed a high-fat diet and anti-miR and control treatments were continued (twice a week *s.c.*) for two weeks. (a) Aortic trees including the carotids were dissected and examined by bright field imaging and lesion area was quantified in (d) n=10 each, data shown as mean ± s.e.m; * $p<0.05$ as determined by 1-way ANOVA). Scale bar =1mm. (b) Frozen sections prepared from the middle parts of these arteries, noted by red arrows in (a) were stained with Oil-Red-O and plaque size was quantified in (e) (n=10 each, data shown as mean ± s.e.m; * $p<0.05$ as determined by 1-way ANOVA). Scale bar =200μm. (c) Representative confocal imaging

of frozen sections immunostained with CD45 antibody is shown (n=10). Scale bar =20μm. For chronic study, *ApoE*$^{-/-}$ mice were fed western-diet (without any partial ligation surgery) and were treated with anti-miR-712 (5 mg/kg, twice a week, *s.c.*) or mismatched control for 3 months (n=10 each). (f) Aortic trees were dissected and examined by *en face* Oil-Red-O staining and the lesion area was quantified in (h) n=4–6 in each group, data shown as mean ± s.e.m; * $p<0.05$ as determined by Student's *t*-test). Scale bar =2mm. Some aortic arches were longitudinally sectioned and stained with Oil-Red-O (g) and plaque size was quantified in (i) (n=4 each, data shown as mean ± s.e.m; * $p<0.05$ as determined by Student's *t*-test). Scale bar =2mm. (j) For TIMP3 overexpression, *ApoE*$^{-/-}$ mice were injected once with AdTIMP3 (10^8 pfu/animal, via tail vein) or control virus (RAD60, 10^8 pfu/animal) 5 days before partial carotid ligation and high fat diet for 2 weeks. (j) Aortic trees including the carotids were dissected and examined by bright field imaging and lesion area was quantified in (k) (n=5, data shown as mean ± s.e.m; * $p<0.05$ as determined by Student's *t*-test). Scale bar =1mm.

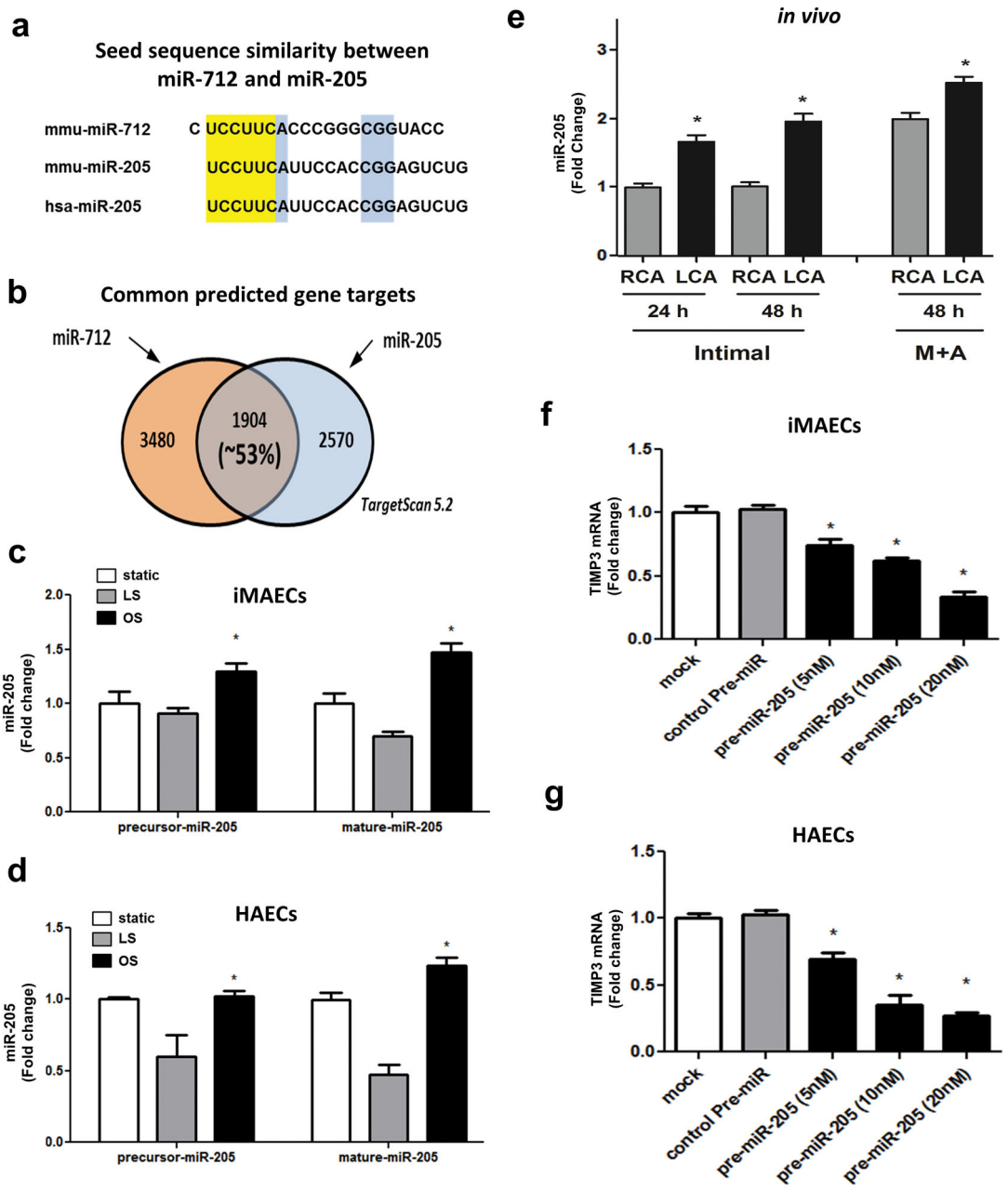

Figure 7. miR-205 is a flow-sensitive human homolog of murine miR-712

(a) The highlighted region in yellow shows the seed sequence match between the murine miR-712 and murine and human miR-205 and those shown in blue indicate additional conserved sequences. **(b)** The putative targets of miR-712 and miR-205 obtained from TargetScan were compared. Venn diagram depicts the common gene targets of miR-205 and miR-712. **(c)** Expression of precursor- and mature miR-205 in iMAECs exposed to static, LS or OS for 24 h (n=4; data shown as means ± s.e.m; *, $p<0.05$ as determined by Student's *t*-test). **(d)** Expression of precursor- and mature miR-205 in human aortic endothelial cells (HAECs) exposed to static, LS or OS for 24 h (n=4; data shown as means ± s.e.m; *, $p<0.05$ as determined by Student's *t*-test). **(e)** Expression of mature-miR-205 was determined using

the RNAs obtained from the endothelial-enriched (intimal region) and the leftover medial and adventitia region (M +A) of the LCA and RCA at 24 h and 48 h post-partial ligation, respectively. Expression of *TIMP3* was determined by qPCR in (f) iMAECs and **(g)** HAECs transfected with increasing concentrations of pre-miR-205 or control-pre-miR compared to vehicle controls (mock) (n=3; data shown as means ± s.e.m; * *, $p<0.05$ as determined by Student's *t*-test).

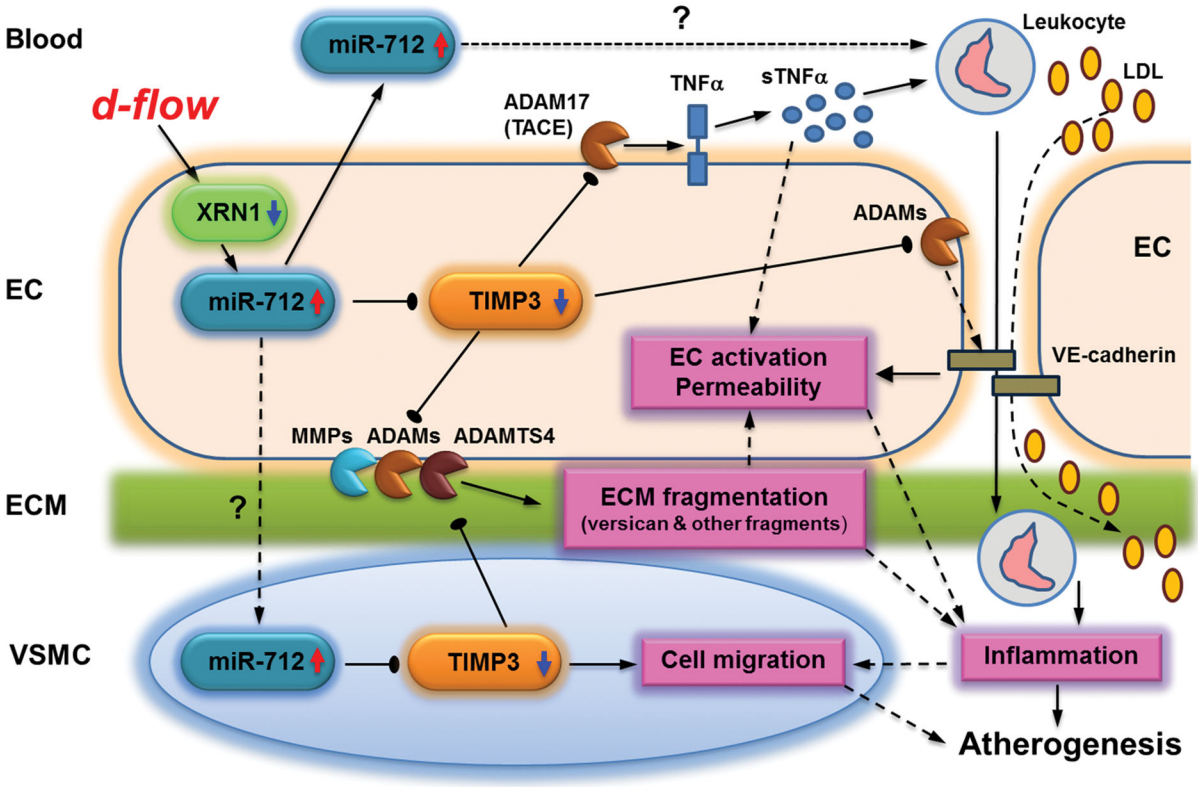

Figure 8. Summary and working hypothesis

miR-712 induces inflammation and atherosclerosis by targeting TIMP3. *D-flow* stimulates miR-712 expression in endothelium by an XRN1-dependent mechanism. Increased miR-712 stimulates endothelial inflammation, permeability and ECM fragmentation by downregulating TIMP3, which is a critical inhibitor of matrix metalloproteinases (MMPs and ADAMs). Decreased TIMP3 expression by miR-712 induces inflammation and atherosclerosis by activating a multitude of metalloproteinases: (1) ADAM17/TACE which releases soluble-TNFα that may induce local and systemic inflammation; (2) ADAMs that shed junctional VE-cadherin, increasing permeability that facilitates LDL and leukocyte infiltration; (3) ADAMTS leading to versican fragmentation; (4) MMPs leading to ECM degradation leading to vessel wall remodeling. Additionally, miR-712 expression is also increased in whole blood and vascular smooth muscle cells (VSMCs) suggesting either transfer of miR-712 from endothelium to these compartments or increase its local production in these compartments. Increased miR-712 in VSMCs induces their migration while circulating miR-712 may affect blood leukocytes further contributing to atherogenesis.